PLOS Biology

RESEARCH ARTICLE

# Single-nucleus transcriptomics of wing sexual dimorphism and scale cell specialization in sulphur butterflies

**Ling S. Loh[1]*, Joseph J. Hanly[1,2,3], Alexander Carter[1], Martik Chatterjee[4], Martina Tsimba[1], Donya N. Shodja[1], Luca Livraghi[1], Christopher R. Day[1,5], Robert D. Reed[4], W. Owen McMillan[2], Gregory A. Wray[3], Arnaud Martin[1,2]***

**1** Department of Biological Sciences, The George Washington University, Washington, DC, United States of America, **2** Smithsonian Tropical Research Institute, Gamboa, Panama, **3** Duke University Department of Biology, Duke University, Durham, North Carolina, United States of America, **4** Department of Ecology and Evolutionary Biology, Cornell University, Ithaca, New York, United States of America, **5** Epigenetics and Stem Cell Biology Laboratory, National Institute of Environmental Health Sciences, Research Triangle Park, Durham, North Carolina, United States of America

* lingsloh@gwu.edu (LSL); arnaud@gwu.edu (AM)





**Citation:** Loh LS, Hanly JJ, Carter A, Chatterjee M, Tsimba M, Shodja DN, et al. (2025) Single-nucleus transcriptomics of wing sexual dimorphism and scale cell specialization in sulphur butterflies. PLoS Biol 23(6): e3003233. https://doi.org/10.1371/journal.pbio.3003233

**Academic Editor:** Abderrahman Khila, Centre National de la Recherche Scientifique, FRANCE

**Received:** November 9, 2024

**Accepted:** May 28, 2025

**Published:** June 18, 2025



**Data availability statement:** Data Files (Data 1–10) all material necessary for reproducibility are available at the Open Science Framework Repository: https://osf.io/yjvkc/(doi:10.17605/OSF.IO/YJVKC). Raw sequencing reads of all experiments are available on the NCBI SRA as listed in the relevant Methods sections.

## Abstract

The evolution of sexual secondary characteristics necessitates regulatory factors that confer sexual identity to differentiating tissues and cells. In *Colias eurytheme* butterflies, males exhibit two specialized wing scale types—ultraviolet-iridescent (UVI) and spatulate scales—which are absent in females and likely integral to male courtship behavior. This study investigates the regulatory mechanisms and single-nucleus transcriptomics underlying these two sexually dimorphic cell types during wing development. We show that *Doublesex* (*Dsx*) expression is itself dimorphic and required to repress the UVI cell state in females, while unexpectedly, UVI activation in males is independent from *Dsx*. In the melanic marginal band, *Dsx* is required in each sex to enforce the presence of spatulate scales in males, and their absence in females. Single-nucleus RNAseq reveals that UVI and spatulate scale cell precursors each show distinctive gene expression profiles at 40% of pupal development, with marker genes that include regulators of transcription, cell signaling, cytoskeletal patterning, and chitin secretion. Both male-specific cell types share a low expression of the *Bric-a-brac* (*Bab*) transcription factor, a key repressor of the UVI fate. Bab ChIP-seq profiling suggests that Bab binds the *cis*-regulatory regions of gene markers associated to UVI fate, including potential effector genes involved in the regulation of cytoskeletal processes and chitin secretion, and loci showing signatures of recent selective sweeps in a UVI-polymorphic population. These findings open new avenues for exploring wing patterning and scale development, shedding light on the mechanisms driving the specification of sex-specific cell states and the differentiation of specialized cell ultrastructures.

**Funding:** This work was supported by the National Science Foundation (IOS-2110532 to WOM, IOS-2110533 to GAW, IOS-2110534 to AM, IOS-2128164 to RDR), the Wilbur V. Harlan Foundation (Wilbur V. Harlan Research Fellowship to MT, LSL, and AC), and the Smithsonian Institution (Postdoctoral Fellowship in Biodiversity Genomics to JJH). The funders had no role in study design, data collection and analysis, decision to publish, or preparation of the manuscript.

**Competing interests:** The authors have declared that no competing interests exist.

**Abbreviations :** ChIP, chromatin-immunoprecipitation; DsiRNAs, Dicer-substrate siRNAs; HCR, Hybridization Chain Reaction; mtDNA, mitochondrial DNA; PBS, phosphate-buffered saline; siRNAs, short-interfering RNAs; SOP, Scale Organ Precursor; UVI, ultraviolet-iridescent.

## Introduction

Animal traits involved in sexual function often differ between the males and females of a given species. The emergence of these sexual dimorphisms from a shared genome implies the existence of regulatory mechanisms that provide cells and tissues with a sexual identity during development. In insects, this somatic sexual identity is primarily acquired in a cell-autonomous fashion, with each cell genotype or karyotype (sex chromosome composition) establishing somatic sex identity via one of many sex determination pathways [1–4]. These diverse genetic cascades generally converge on a shared integrating mechanism across insects, the differential splicing of sex-specific isoforms of the *Doublesex* (*Dsx*) pre-mRNA, resulting in transcription factors called DsxM in males and DsxF in females [5–7]. Comparative studies of *Dsx* indicate that its expression is often spatially restricted to cells with dimorphic potential, including in gonadal tissues, epithelial structures, and neuronal circuits [8–17]. DsxM and DsxF share similar occupancy profiles across the *Drosophila* genome, suggesting that the majority of their binding targets are not sex-specific [18,19]. Instead, DsxM and DsxF may mediate distinct, and sometimes opposite *cis*-regulatory effects to bias gene expression. For example, in the *Drosophila melanogaster* abdomen, DsxM represses the BTB-domain transcription factor gene *Bric-a-brac* (*Bab*), while DsxF activates it [20,21]. As Bab represses dark melanization in the fly abdomen, this dual regulation underlies the dichromatism of *D. melanogaster* where only males are fully pigmented in their last two abdominal segments.

To understand how somatic cell identity is integrated into dimorphic gene expression programs, we can leverage the study of scale cell precursors that underlie sexual dichromatism in butterflies. Each color scale is the extension of a single cell, and each cell integrates spatial and sexual cues during development to differentiate into the biological pixels that form wing patterns. The Orange Sulphur butterfly *Colias eurytheme* is an emerging model system for the study of scale dimorphism [22–26]. Not only do the males and females of this species show distinct melanic patterns on their dorsal wing surfaces, but males also exhibit a bright ultraviolet-iridescent (UVI) pattern that is used as a species recognition signal by conspecific females to avoid interspecific matings [27–31]. UV-iridescence is conferred by the specialization of their dorsal cover scales, which form dense stacks of 7–9 air-chitin layers on their upper surface in males. Females lack UVI scales and instead show typical orange scales, which do not elaborate a multilayered ultrastructure. The butterfly ortholog of *Bab* is expressed in most scales, where it represses the UVI trait [29], but it is specifically silenced in the male dorsal cover scales starting at 35% of pupal development, thus activating UVI fate in males by derepression. Hybrid males carrying at least one *Bab* allele from *Colias philodice,* a monomorphic, non-UVI species, express Bab in their dorsal cover scales and lack UVI scales. In summary, Bab is both necessary and sufficient to block the terminal differentiation of UVI scales, and *C. eurytheme* alleles of *Bab* turn off its expression in male dorsal cover scales, thus activating the UVI state by derepression.

To understand the mechanism of sexual differentiation in the butterfly wing, it is also important to place scale differentiation into a broader developmental context.

The pupal wing of lepidopteran insects consists of an epithelial bilayer, where dorsal and ventral surfaces are separated by an acellular baso-lateral membrane. The structural integrity of this tissue is maintained by small columnar epithelial cells. Scales are macrochaetes that derive from the differentiation of a Scale Organ Precursor (SOP) cell lineage, akin to mechanosensory bristles [32,33], that prevent the forming of associated neurons and glia to only give rise to a trichogen (scale) cell precursor and an associated tormogen (socket) cell [34–37]. Scale cell precursors become large, polyploid, and aligned along tightly arranged rows that alternate between cover scales, that will give rise to scales on the top surface, and a lower layer of ground scales [38–40]. Pupal wings are also infiltrated by trachea, including major branches and numerous small tracheoles that transiently invade the wing epithelium during early pupal development [41,42]. The major branches develop inside the lumen of epithelial tubes that persist into sclerotized wing veins, which provide robustness to the adult wing and act as a hemolymph circulatory system [43]. Finally, the pupal wing is embedded with mobile hemocytes [41,42], and likely contains a small population of neuroglial cells due to the presence of mechanosensory and thermosensitive sensilla, particularly along the wing veins [43].

Here, we delve into the cell type diversity of the developing wings of *C. eurytheme,* with the overarching goal of linking gene expression programs and the sex-specific differentiation of complex scale ultrastructures, such as the UVI scales found in males. First, we test the effect of *Dsx* loss-of-function in wing development in both sexes to infer its roles in sexual dimorphism. Second, we analyze the single-nucleus transcriptome of a male developing wing and profile gene expression in scale cell precursors at a cellular resolution, with a focus on differentiated clusters that correspond to two male-specific, specialized cell types. Last, we integrate transcriptome signatures with ChIP-seq profiles of Bab occupancy to sketch a set of potential Bab transcriptional targets involved in UVI scale differentiation. Overall, this study illustrates how color scale types emerge from divergent gene expression programs, and provides foundational knowledge for the study of sexually dimorphic cell types.

## Results

### Two male-specific scale types with divergent ultrastructures

The sexual dimorphism of *C. eurytheme* butterflies manifests on the dorsal surface of their wings, where males show bright UV iridescence across the medial orange region, as well as a thin, continuous marginal black band (Fig 1A). There is no UV-iridescence in wild-type females, and their marginal patterns are wider, jagged at their interface with the orange area, and flecked by yellow spots (Fig 1A). The two sexes thus differ in UV-iridescence as well as in the morphology of the marginal band. We used Scanning Electron Microscopy to further survey the ultrastructure of scale types in *C. eurytheme* (Fig 1B–1H). Typical scales that are found on either sex or wing surface share a 2-μm distance between their apical ridges (2.0 ± 0.1 μm, $N = 125$ measured scales), a feature that is relatively constant across melanic scales (*e.g.,* forewing discal spots of both sexes), pterin-pigmented scales (orange, yellow), and pterin-deficient scales (*e.g.,* white scales from Alba female morphs). In contrast, UVI scales are not only characterized by the multilayering of their ridge lamellae [23,29,44], but also by the density of the ridges themselves, with a distance between ridges averaging only 1 μm (1.0 ± 0.1 μm, $N = 25$ scales) (Fig 1D, 1G). A second type of male-specific scale type, here dubbed the spatulate scales, show a large inter-ridge distance of 4.4 ± 0.5 μm ($N = 20$ scales) that gives them a corrugated look under light microscopy. These scales have an unusual ultrastructure, with crossribs that resemble soybean pods joining the longitudinal ridges (Fig 1D, 1H), and that overlay a porous inner matrix [45]. It was proposed that these scales play a role in pheromone retention or spreading, due to their male-specificity and the spongy aspect of their ultrastructure [27,46,47]. Spatulate scales occur specifically on the cover scale layer of the male melanic bands, where their wide apical lobes overlay a layer of yellow ground cover scales. In females, the dorsal marginal band is devoid of spatulate scales and shows instead canonical melanic scales as cover scales. In summary (Fig 1I, 1J), the dorsal surface of *C. eurytheme* wings includes two male-specific scale types that each feature unique ultrastructures—the UVI scale and spatulate scales.

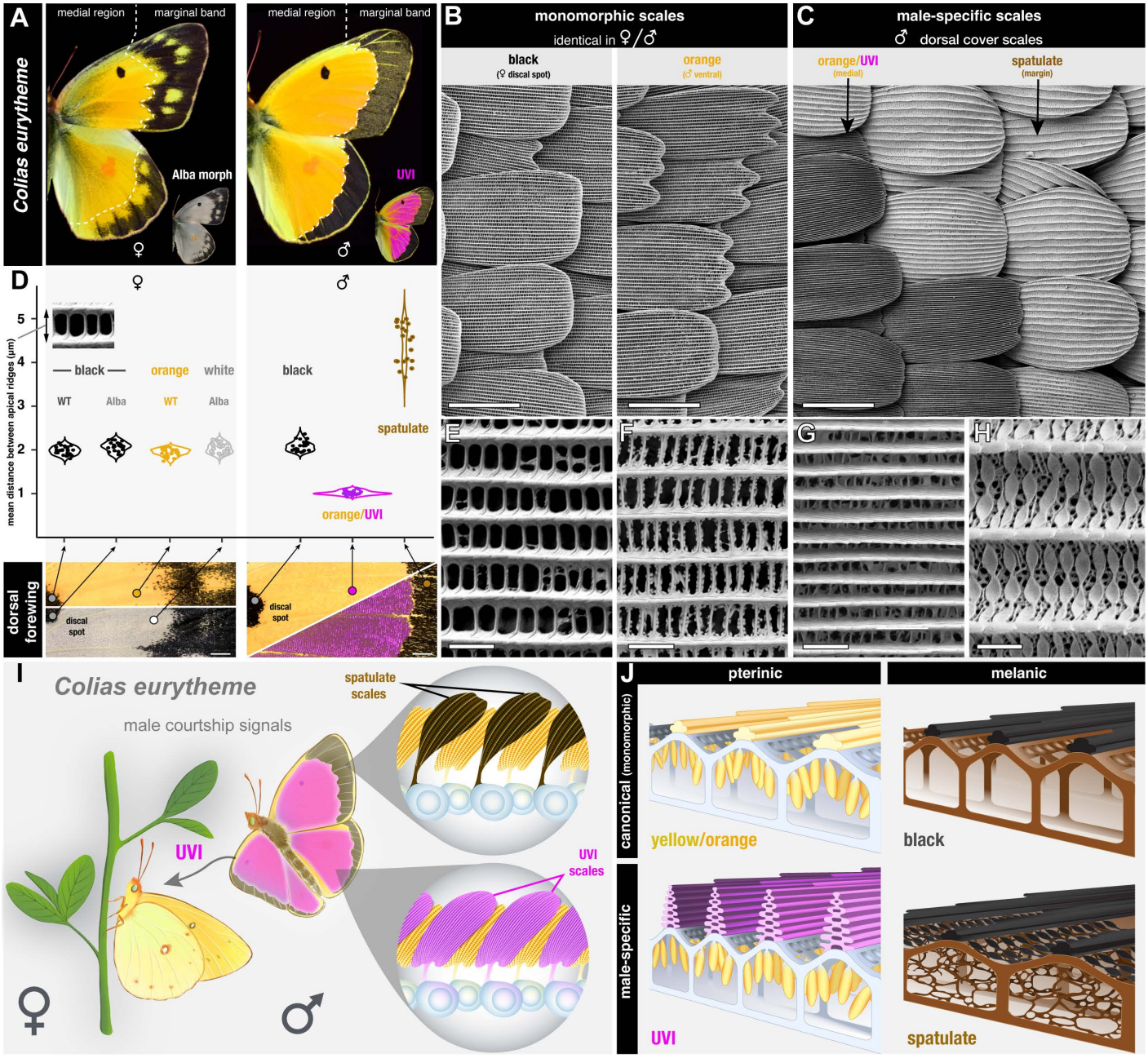


**Fig 1. Male-specific scales in the dorsal wings of *Colias eurytheme*.** **A.** Dorsal views of male and female butterflies, highlighting the difference in width and patterning of the marginal bands, and the male-specific UV-iridescence (magenta; an UV-photograph was colored in magenta and overlaid on a normal image). Alba morphs are a female-limited phenotype characterized by pterin-pigment deficiency in their scales. **B, C.** Scanning electron micrographs of representative non-dimorphic scales (here in B, left: female dorsal forewing melanic scales of the discal spot; right: male ventral orange scales), and male-specific scales (here in C: interface between UVI and spatulate scales, dorsal hindwing). **D.** Mean apical ridge distance in individual scales from melanic discal spots, medial regions, or male marginal bands, highlighting the derived ultrastructure of male-specific UVI and spatulate scales. Each category features $N = 25$ scales—except for spatulate scales ($N = 20$). The measurements originate from electron micrographs of dorsal wing surfaces in a total of three individuals: an orange female, an Alba female, and a male (Supplementary Methods in S1 Text and Data 10 at https://osf.io/yjvkc/). **E–H.** Apical views of the ultrastructure of representative scale types (same scale types as in panels B, C), featuring the longitudinal ridges (horizontal structures) and the transversal microribs (vertical). **E**: female dorsal cover black scale; **F**: male ventral cover scale (orange, non-UVI); **G**: male UVI dorsal cover orange scale; **H**: male spatulate dorsal cover margin scale. **I.** Position of male-specific cell types on the dorsal wings. The cell bodies of scale precursors (blue) are transient structures that do not occur in adults. **J.** Schematic representation of the ultrastructures (viewed as transversal cross-sections) from the four main scale types—canonical (orange and black), UVI, and spatulate. Scale bars; B and C = 50 µm; D = 1 mm; E–H = 2 µm.

https://doi.org/10.1371/journal.pbio.3003233.g001

### *Doublesex* has distinct functions on marginal patterning and UV dichromatism

Gene loss-of-function assays targeting *Dsx* generate intersexual phenotypes across insects, with secondary sexual characteristics losing their sex-specific differentiation, and sometimes reversing to the state found in the opposite sex [9,48–53]. We thus used CRISPR-targeted mutagenesis to generate $G_0$ adults carrying *Dsx* mosaic knock-outs (abbreviated mKO, or "crispants"), using single sgRNAs that targeted either the DNA-binding Domain or the Dimerization Domain shared across *Dsx* isoforms [6], resulting in deletion alleles at the target sites (S1 Fig). *Dsx* crispant adults showed mosaic effects on sexually dimorphic features of the dorsal wings (Fig 2, S1 Table). Of note, $G_0$ crispant wings are mosaics of tissues carrying *Dsx*-deficient and wild-type cells, and while 33 crispant individuals showed spatially variegated effects as a result of this mosaicism, these experiments yielded consistent effects within each sex (S2, S3 Figs). *Dsx* crispants from both sexes showed intermediate intersexual states in the aspect of the marginal bands, the melanic patterns at the distal edge of their wings. The marginal bands of female crispants showed a narrowing of the melanic marginal band compared to wild-type females, resulting in a loss of yellow spots. The reverse was observed in the marginal bands from male crispants, with a partial expansion of the melanic band resembling the female state.

The effects of *Dsx* mKOs on UV-iridescence indicated two distinct categories of effects between males and females. Female crispants showed a gain of UVI that phenocopies the male state (Fig 2A–2C′). This conversion towards UVI scale types occurred along sharp clone boundaries (Fig 2D), showing that DsxF is necessary for the repression of UVI in cell autonomous fashion. In contrast, while male crispants show a spatial reduction of the UVI field (Fig 2A, 2B), neither these UVI-loss effects showed sharp clonal boundaries that would indicate autonomy, nor did these effects extend into the proximal and central sections of the wing (S2 Fig). This indicates a shift in the positioning of pattern boundaries in the vicinity of the marginal region (Fig 2C–2C′), likely due to non-autonomous effects on morphogenetic signaling in this region. In addition, we introduced short-interfering RNAs (siRNAs) via electroporation to drive RNAi knockdowns of *Dsx* at the pupal stage [10,54]. UVI scales were unaffected throughout the central domain of the RNAi-treated male dorsal forewings (Fig 2E). Consistent with the mosaic knock-outs, female wings electroporated with *Dsx* siRNA showed ectopic UV-iridescence in the cover scales (Fig 2E, 2F). To explain these non-autonomous effects in males, we extrapolate that the spatial patterning of the marginal region includes sex-specific inputs on morphogenetic signaling events, that in turn determine its width and sub-division into fields of melanic *versus* non-UVI yellow scales.

### DsxF activates Bab expression in female dorsal cover scales, repressing UVI scale identity

Both *Dsx* KOs and knock-downs result in ectopic UV iridescence across the female medial region, and conversions to the UVI scale type are restricted to cover scales (Fig 3A, 3B). This cover scale specificity is unlike the effect of *Bab* KOs [29], which converts both the ground and cover scale layers to a UVI state. Next, we profiled the expression of Dsx between 30%–40% of pupal development—a temporal window where Bab becomes downregulated specifically in male UVI scale cells. To do this, we used a monoclonal antibody that recognizes the Dsx-DBD (DNA-binding domain) shared by both isoforms [55–57]. Because Dsx isoforms are sex-specific in Lepidoptera, for simplicity, we call the detected antigen DsxF or DsxM based on the sex of the dissected pupae. In females, DsxF is detected in both cover and ground scales throughout the entire wing (Fig 3C), like Bab (Fig 3C′). In contrast, DsxM is only expressed in the dorsal cover scales of the wing margin in male wings (Fig 3D–3D′). This absence of DsxM in the medial region explains why its perturbation does not result in autonomous loss of UVI scales in males.

Next, we tested the regulatory interaction between DsxF and Bab by examining Bab expression in female wings knocked-down for *Dsx*. While the contralateral, untreated controls from the same individual show expression of Bab in both dorsal ground and cover scales at the 40% stage, Bab expression is low or undetectable in dorsal cover scales in the wings electroporated with *Dsx* RNAi, taking an alternating configuration (Fig 3E, 3F). In other words, *DsxF* is required to maintain Bab expression at high levels in the female dorsal scale, thus feminizing the wing phenotype by preventing UVI scale differentiation.

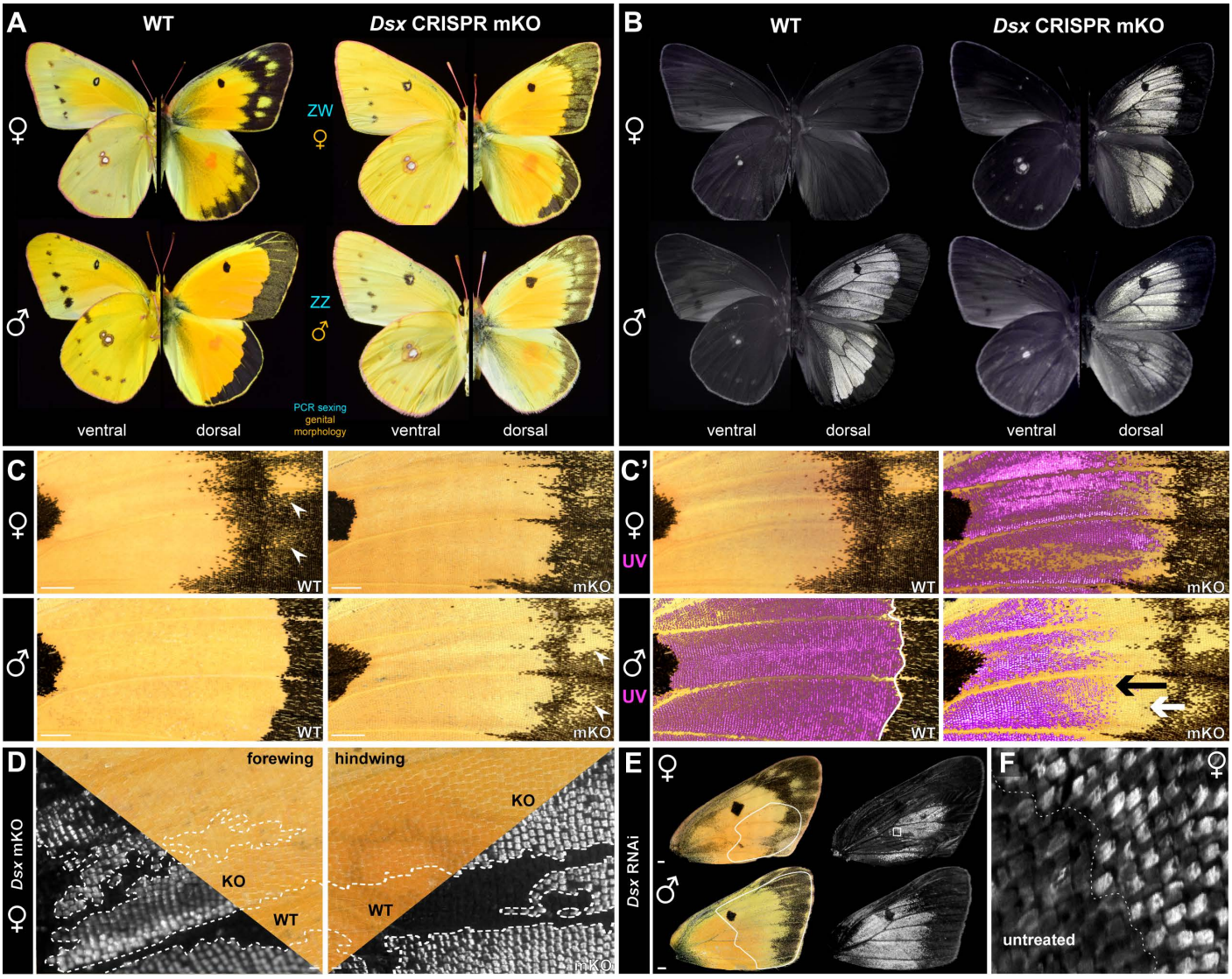


**Fig 2. *DsxF* blocks UV-iridescence in females in a cell-autonomous fashion. A.** Effects of *Dsx* mosaic knock-outs (mKO), as seen in comparisons of female and male WT individuals with representative *Dsx* $G_0$ crispants. The sex of each crispant was determined by concordant genital morphology and genotyping. Phenotypic effects are limited to the dorsal surfaces and most visible in the marginal region. **B.** UV-photography (320–400 nm) of UV-iridescent dorsal patterns in the same mutants, showing an ectopic gain of UVI scales in females (top). In males (bottom), the feminization of the marginal region triggers a regression of the male UVI pattern distal border. **C–C′.** Close-up views of the central forewing regions (same individuals as in panels A, B), including overlays of UV photographs (C′: magenta false-color) over visible light images, and highlighting the intermediate states of marginal patterns. In females: gain of UVI scales, regression of the melanic marginal patterns. In males: gain of female yellow spots in males (arrowheads), extension of the melanic marginal patterns (white arrow), and regression of the UVI field (black arrow). **D.** Cell autonomy of UVI scale gains in female *Dsx* mKOs, as shown by continuous UVI mutant clones with sharp boundaries (KO). Superimposed views of the same region, taken in visible and ultraviolet light, are shown across each diagonal line. **E.** RNA interference effects of *Dsx* siRNA electroporation in male and female forewings. Dotted lines mark the approximate areas that were electroporated. *Dsx* knockdown results in ectopic UVI (top), and in a feminization of the marginal pattern in males, including with a regression of medial UV iridescence at its distal border. F. High-magnification view of the female wing shown in panel E, at the interface of the treated (ectopic UVI scales) and untreated area. Scale bars: C, E = 1 mm; D = 100 μm.

https://doi.org/10.1371/journal.pbio.3003233.g002

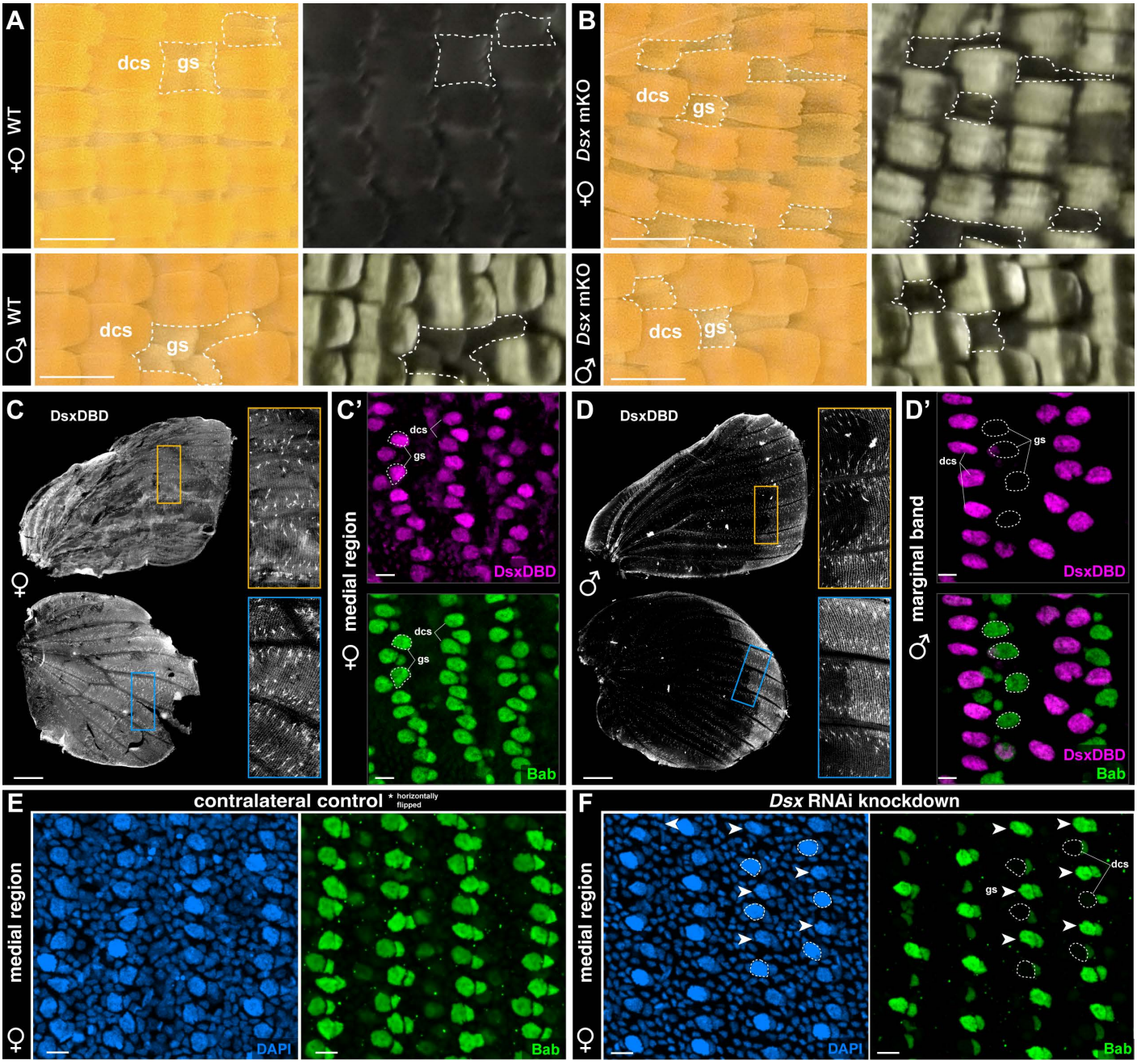


**Fig 3. DsxF medial expression activates Bab in the female dorsal cover scales. A, B.** High-magnification views of central dorsal wings, showing dorsal cover-scale (dcs) specific transformation of non-UVI to UVI scales in female *Dsx* KOs. Males are unaffected by *Dsx* mKOs in the central region. Dashed lines indicate small patches of the wing where ground scales (gs) are exposed. **C–D′**. Immunofluorescent detection of the DsxDBD antigen in the dorsal layer of female and male wings between at 40% of development. The Bab antigen (green) marks both dorsal cover scales (dcs) and ground scales (gs) in females (C′), and only the ground scales in males. Forewings are shown in C′ and D′ insets. **E, F.** Immunofluorescence of Bab (green) in the control (E, contralateral left wing, horizontally flipped for re-orientation) and treated (F) female forewings following electroporation with *Dsx* siRNAs, shown at the 40% pupal stage. DAPI DNA stainings (blue) highlight rows of scale nuclei interspersed by smaller epithelial nuclei. *Dsx* RNAi results in loss of Bab expression in dorsal cover scales (dcs, dotted lines), while maintaining Bab expression in ground scales (gs, arrowheads). Scale bars: A, B = 100 μm; C, D = 1 mm; C′, D′, E, F = 10 μm.

https://doi.org/10.1371/journal.pbio.3003233.g003

### Dsx controls the sex-dependent identity of margin cover scales

While Dsx is expressed in all the scale cell types of the marginal region in females, it marks dorsal cover scales in the marginal region of males. Marginal dorsal scale cells are sexually dimorphic, with a canonical melanic type in females versus the derived spatulate type in males. Accordingly, *Dsx* CRISPR KOs showed complete reciprocal transformation of the melanic dorsal cover scales between these marginal/dorsal scale types between sexes, from canonical melanic to spatulate in *DsxF* mKOs, and vice-versa from spatulate to canonical in *DsxM* crispants (Figs 4A–4C and S4). Thus, while only *DsxF* is required for specifying the UV dichromatism, both *Dsx* isoforms are required to instruct the correct patterning of marginal patterns and the identity of male-specific scales within them.

### The combinatorial logic of dimorphic scale type specification

We summarize below how Dsx controls multiple aspects of sexual dimorphism on the dorsal wing (Fig 5A). The spatial expression of *Dsx* is sexually dimorphic at the 30%–40% pupal stage: female wings express DsxF in all scales, while males only express DsxM in the dorsal cover scales of the marginal region. Dsx influences the patterning of the marginal band via non-autonomous effects, determining the spatial extent of the melanic band and of non-UVI yellow outlines and spots. The differences in spatial localization of Dsx sexual isoforms likely explain the asymmetric effects of its perturbation in each sex. In the medial region, DsxF is required to feminize dorsal cover scales, by repressing UVI states. In the wing margin, sex-specific Dsx isoforms are required to feminize dorsal cover scales into a canonical melanic type or to masculinize them into the spatulate type.

Next, we developed a phenomenological model that integrates the effects of Dsx and Bab on male-specific cell type specification. We replicated the effects of *Bab* mKOs [29] using RNAi knockdowns targeting the dorsal surface of the forewings from each sex, and summarized the observations from both sets of perturbation experiments (Fig 5B–5D). In females, Bab-deficient cells all acquire a UVI-scale morphology including UV-iridescence and high ridge density. Because all the female scale cell precursors express Bab (S5 Fig), this is visible in both cover and ground scales of both the medial

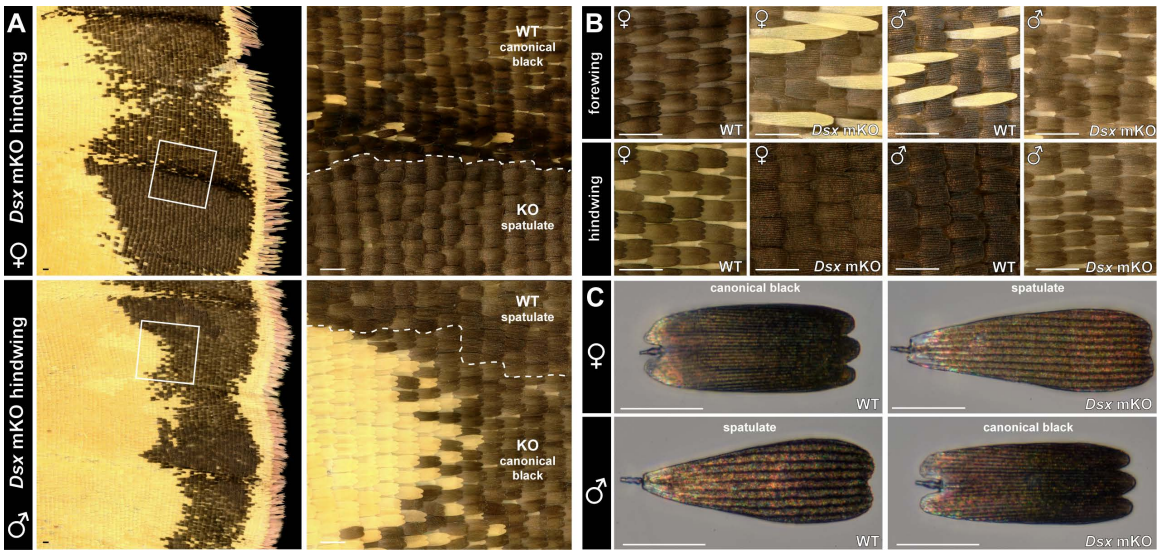


**Fig 4. Doublesex controls the specification of male-specific spatulate scales. A.** Magnified views of the dorsal hindwing marginal bands of mosaic *Dsx* $G_0$ crispants. KO clone boundaries are visible with yellow/orange color shifts in the medial region, and in the marginal band, with shifts from canonical black scales to the spatulate scales in females, and vice-versa in males. **B, C.** Complete, reciprocal shifts in scale composition (B) and melanic scale identities (C) in both female and male *Dsx* crispants. Scale bars: A–C = 100 μm.

https://doi.org/10.1371/journal.pbio.3003233.g004

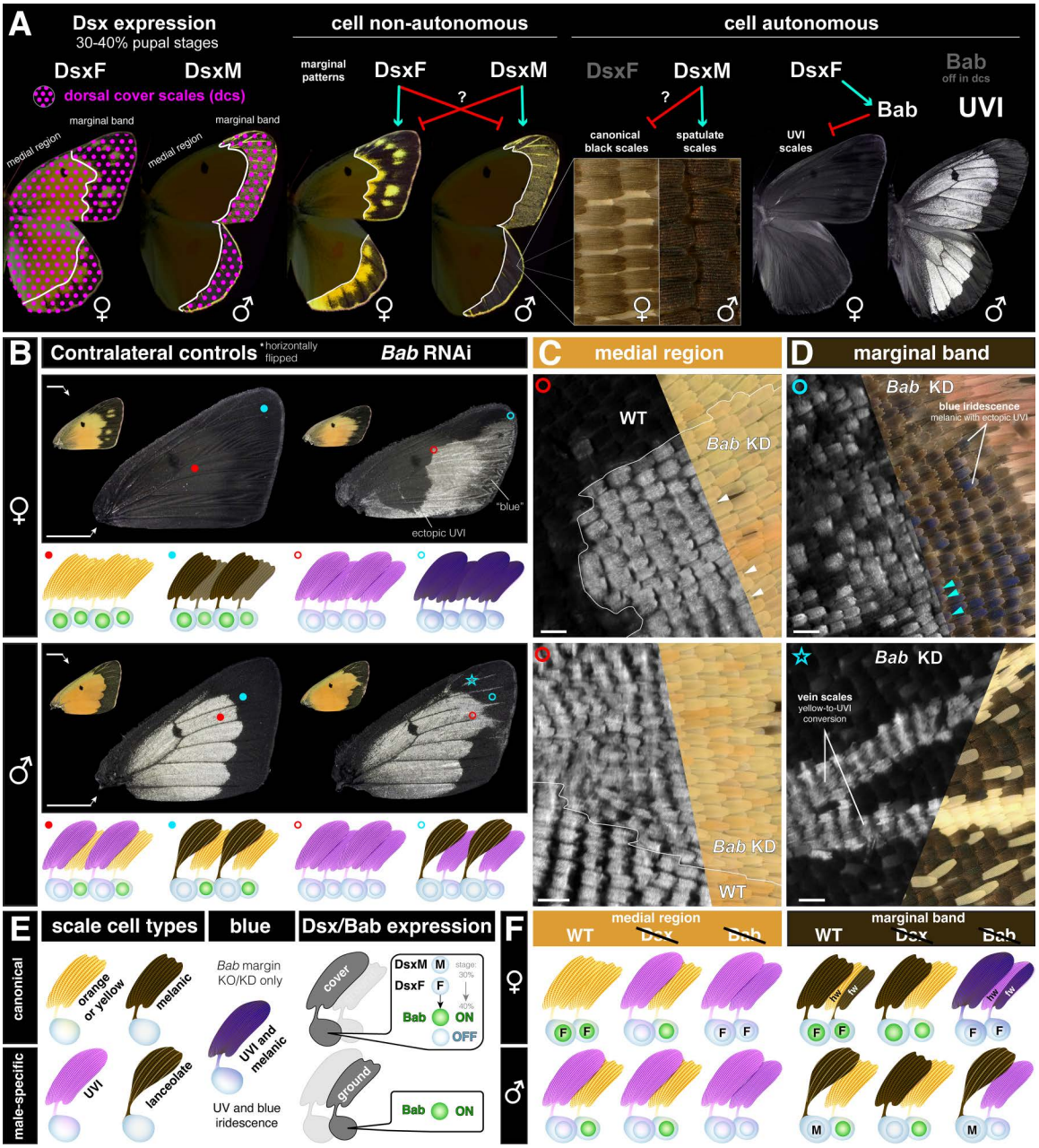


**Fig 5. Dsx and Bab control sexually dimorphic scale fates. A.** Working hypothesis for the effects of *Dsx* on sexually dimorphic wing traits, including cell non-autonomous patterning effects on marginal patterns, cell-autonomous requirements in the specification of spatulate *vs.* canonical margin scales, and female-specific repression of UV-iridescence in dorsal cover scales. **B–D.** *Bab* RNAi knockdowns on the dorsal forewing phenocopy mosaic KO effects [29]. Bab-expressing cells acquire a UVI state upon *Bab* perturbation, with the exception of the spatulate scales that are unaffected. This includes canonical melanic scales that acquire UV-iridescence while maintaining melanism (D, cyan arrowheads), resulting in a dark blue iridescent phenotype in the visible spectrum (panel D), as previously described in *Bab* mosaic KO experiments [29]. Ground scales are transformed to yellow UVI scales in each sex (*e.g.,* in the medial region: C, white arrowheads), except in the female forewing marginal band where they convert from melanic to blue iridescent (combination of melanic and UVI features). Star: inset features yellow vein scales (UV-negative in WT and controls) that acquire a UVI fate upon Bab RNAi, indicating successful knockdown in this area. **E, F.** Summary of Dsx expression, Bab expression, and perturbation assays in dorsal wing surfaces. Scale bars: B = 5 mm; C, D = 100 μm.

https://doi.org/10.1371/journal.pbio.3003233.g005

and marginal regions. In the marginal region, UVI scales retain a melanic state, and the combination of UVI-structural and melanic features confers them a dark blue iridescence, visible with the naked eye when illuminated with a low angle of incidence, as previously observed in female Bab mKOs [29]. In males, only ground scales express Bab, and accordingly, *Bab* perturbation results in ground scale-specific conversions to UVI states. These knockdown effects confirm that Bab inhibits UVI trait differentiation and that this occurs during pupal stages. Bab does not appear to control other aspects of sexual dimorphism, other than UVI.

Together, these data suggest a combinatorial logic for male-specific cell type specification (Fig 5A, 5E, 5F). Across the entire dorsal wing of each sex, ground scales express Bab and repress UVI without Dsx input. In the medial region, DsxF feminizes the dorsal cover scales by recruiting the UVI-repressing activity of Bab. In marginal regions, DsxF maintains canonical states, while DsxM is specifically expressed in the dorsal cover scales and masculinizes them into spatulate states.

### Overview of cell type diversity in the 40% male pupal hindwing

Our analysis of Dsx shows that male wings differentiate two derived scale types with specialized ultrastructures, the UVI and spatulate scales. Next, we used single-nucleus RNA sequencing (snRNA-seq) to gain further insights into the molecular basis of this diversity of cell types in the male wing. We chose to sequence a hindwing from a *C. eurytheme* male individual at 40% pupal development, a stage where Bab is consistently repressed in the dorsal cover scales that give rise to the UVI state [29]. Quality control showed low-contamination of mitochondrial reads following filtering at the 3% threshold (S6 Fig), resulting in 2,961 filtered cells. Unsupervised clustering yielded nine robust clusters, as visualized here in UMAP reduced-dimensionality space (Fig 6A). We then used the *FindMarkers* function of Seurat version 5 to identify differentially expressed features between these clusters (Data 1 at https://osf.io/yjvkc/), and annotate them based on marker gene enrichment and the known function of their orthologs in *Drosophila*. Two minor clusters, dubbed *Misc1* ($N = 44$ nuclei) and *Misc2* ($N = 35$ nuclei), remain unannotated and will require further work for confident assignment of cell types within them (see Discussion). The seven remaining clusters consist of two epithelial cell types dubbed *Wing_epi* and *Trch_epi*, and five clusters related to SOP subtypes—namely one socket cluster (*Socket*) and 4 scale sub-types (*Scale1* to *Scale4*), as detailed below. Of note, scale cell types showed higher numbers of mapped reads and detected genes compared to non-scale cell clusters (Fig 6B), likely due to differences in ploidy levels. Non-scale cell types also showed a higher level of mitochondrial DNA (mtDNA) contamination relative to scale types (Fig 6C).

The bulk of cells providing structural integrity to the wing surface, to the inner surface of the lacunae (luminal tunnels invaded by trachea), and to the tracheal system are epithelial, diploid cells. Consistent with this, both tracheal (*Trch_epi,* 140 cells) and wing-related (*Wing_epi,* 780 cells) epithelial clusters shared top marker genes that are known epithelial cell markers in flies (Fig 6), such as the protease gene *Stubble* involved wing epithelial remodeling [58], the EGF signaling pathway genes *pointed* and *EGFR* [59], the wing cell polarity factors *fat* and *starry night* [60,61], and the genes *grainy-head*, *headcase* and *blistered* [59,62–65]. *Ultrabithorax* is known as an epithelial marker in butterfly pupal hindwings [39] and was enriched in both epithelial clusters. Notch showed epithelial and socket cell signals consistent with our previous study [37]. In addition to their shared epithelial gene expression profile, the two clusters differ by the expression of markers that are hallmarks of tracheal tip cell growth and tracheal branching, including the tracheal progenitor selector gene *trachealess*, the FGF ligand/receptor pair *branchless*/*breathless*, the proteoglycan *dally* involved in tracheal FGF signaling, and the cytoskeletal factor *Zasp52* [66–69]. It is also noteworthy that some *Trch_epi* markers such as *datilografo*, *APP-like* and *slow border cells* were not expected in a trachea-related tissue based on current knowledge, indicating possible evolutionary divergence with *Drosophila*. Further investigation will be required to refine the range of cellular identities of the *Wing_epi* and *Trch_epi* clusters, for example, to decipher the dynamic complexity of tracheal development, and the differences between wing-membrane and lacunar epithelia in butterflies.

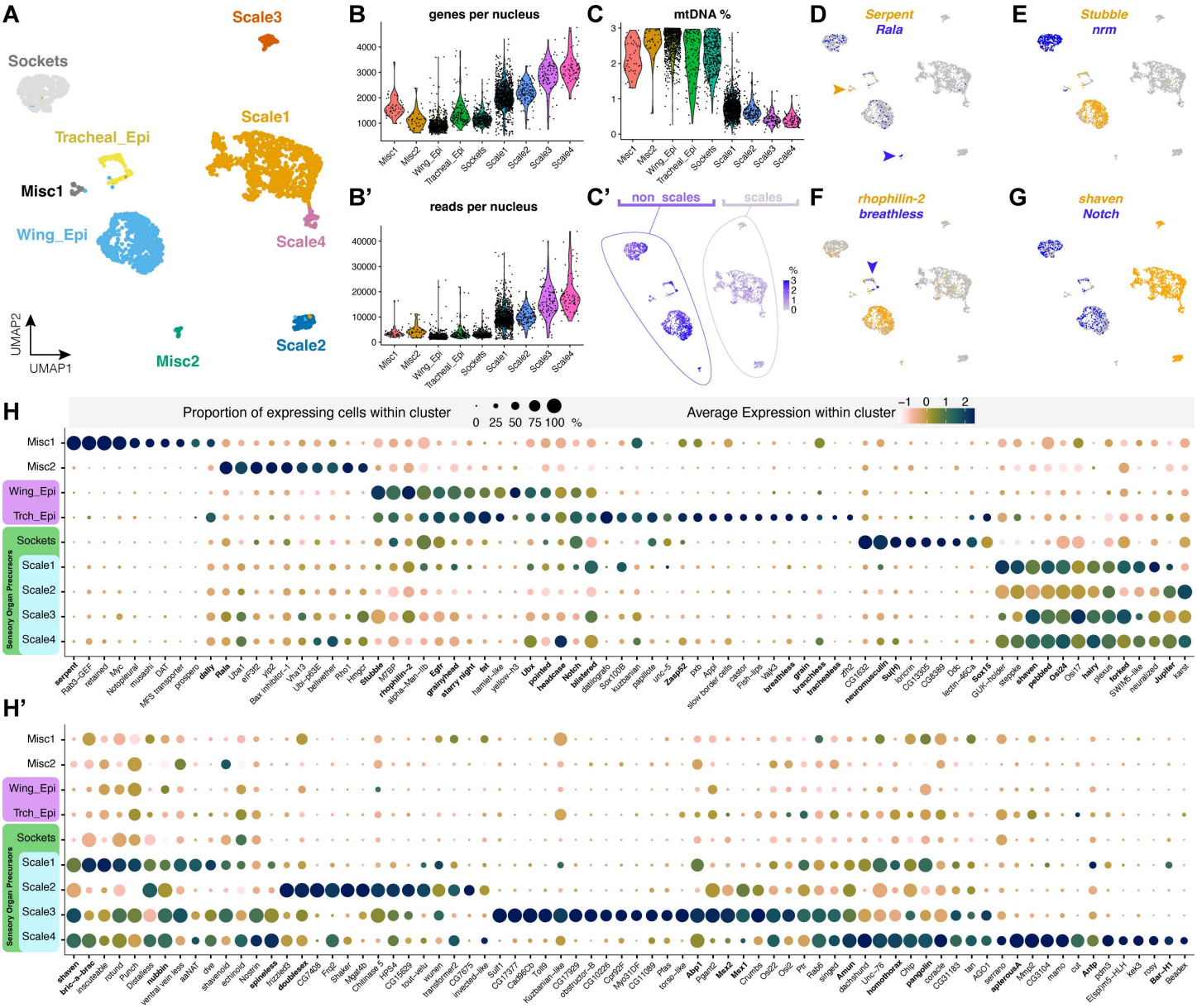


**Fig 6. Single-nucleus transcriptomic profiles of major cell types in the *Colias eurytheme* male 40% pupal hindwing. A.** UMAP plot representing the 9 clusters resolved across a total of 2,961 cells. **B–B′.** Violin plots of the number of unique genes (B) and RNA read counts (B′) per nucleus. **C–C′.** Violin and heatmap plots highlighting differences in mtDNA content across non-scale and scale clusters. **D–G.** Heatmap plots showing the expression of key marker genes (bold: see main text for citations). *Serpent* and *Rala* (arrowheads) in two small unannotated clusters, *Stubble* (epithelial cells), *neuromusculin* (*nrm*, socket cells), *rhophilin-2* (wing epithelium), *breathless* (tracheal epithelium), *Notch* (non-scales), and *shaven* (*sv*, scales). **H–H′**. Dot plots featuring the expression profiles of 150 differentially expressed genes, chosen among top markers of cluster or cell type identity (**Data 1 at** https://osf.io/yjvkc/). Panel H includes top markers for non-SOP clusters, socket cells, and scale cells; panel H′ focuses on differentiators between scale sub-types. Dot size reflects the percentage of cells in which gene expression was detected. Color coding allows a relative comparison of gene expression levels within a cluster (horizontal comparisons), but is not proper for vertical comparisons between clusters. Gene names in **bold**: see main text for references. Feature count matrices and Seurat objects used for the generation of all panels are available at the Open Science Framework Repository [78].

https://doi.org/10.1371/journal.pbio.3003233.g006

Developmental studies have shown that in butterflies, the SOP lineage has fully differentiated into arranged rows of scale and socket pairs by 30% of pupal development [40]. This differentiation was well resolved in the 40% stage single-nucleus transcriptome, with a clear cluster of 412 socket cells, based on the expression of the markers *Su(H)*, *Sox15*, and *neuromusculin* (*nrm*), previously associated with *Drosophila* socket specification [70,71]. A total of 1,550 nuclei from scale-building cells were distributed across four distinct clusters that shared the expression of the trichogen master gene *shaven* (*sv*) [36,72,73]. Scale-related clusters also shared additional marker genes associated with trichogen development in flies such as *pebbled* (*peb*) [74], *Osi24* [75], *Jupiter* [76], and *Amun* [77], supporting the proposed homology between the shaft of mechanosensory bristles with the scale derivative of butterflies and moths [32,34,37]. The next section focuses on refining the divergence between groups of scale cell precursors.

### Transcriptome heterogeneity among scale subtypes in the 40% pupal male hindwing

The preliminary differential expression analysis of whole-wing nuclei suggests that scale cell precursors (*sv*+/*peb*+/*Osi24*+) resolve into at least four subtypes, including the large *Scale1* cluster. To delve into the processes of color scale differentiation, we bioinformatically isolated *Scale1-2-3-4*, re-normalized gene expression counts, and reclustered this subset of nuclei to augment the resolution and separation of scale cell subtypes (Fig 7A). All eight scale clusters expressed canonical scale cell precursor markers such *sv*/*peb*/*Osi24* (Fig 7B). The *Scale1* cluster forms five subclusters numbered *Scale1a* to *1e* for which we have not resolved defined identities at the moment, except for *Scale1d*, which is marked by Antennapedia (Antp) and the pterin repressor Bar-H1 [25] and seemingly encompasses the white scales of the wing coupling region (Fig 7C, 7D). *Scale4* likely corresponds to hairlike scales of the dorsal surface (Fig 7D, 7E), based on the expression of *homothorax* and *apterous-A* [79,80], and immunolocalization of Cut (Fig 7F–7J′). *Scale1b* expresses *nubbin* and may correspond to a ground scale cell type (Fig 7K, 7L).

### UVI and spatulate scale cells are highly differentiated

To further profile the transcriptomes of the two most divergent clusters, we listed 1,006 genes showing significant differential expression (adjusted *p-value* < 0.05; minimum *log2FC* = 1.25; *min.pct* = 0.25) in comparisons between *Scale2*, *Scale3*, and the remaining scale groupings (**Data 2 at** https://osf.io/yjvkc/). Filtering this list down to 145 most statistically significant genes (adj. *p-value* < $10^{-50}$) allows a heatmap visualization of the genes that are depleted or enriched in these clusters compared to other scale types (Fig 8A—8A′). Remarkably, both clusters *Scale2* and *Scale3* share a low expression of the UVI-state repressor Bab, a repressor of the UVI state that is repressed in UVI cells [29]. One of the two clusters thus likely corresponds to UVI scales, and we used fluorescent Hybridization Chain Reaction (HCR) mRNA detection of marker genes to resolve their identity. The snRNA-seq signal for *DsxM* indicates it is enriched in the *Scale2* cluster alongside *Arylsulfatase*, a more specific marker for this cell population (Fig 8B). Both genes showed strong transcript signals in the dorsal margin areas where spatulate scales are located (Fig 8C–8D). *Actin-binding protein 1* (*Abp1*) is a negative marker of *Scale2*, and indeed showed a complementary expression to *Arysulfatase*: while *Abp1* is strongly expressed in the orange/UVI area, this signal decreases in the margin and shows a weak marking of alternating scale cells, as expected from an expression in ground scales (Fig 8D). Meanwhile, the *Scale3* marker gene *Sulfatase1* showed a visible association with the dorsal cover scales of the medial wing area (Fig 8E). Together, these results thus annotate the *Scale2* (*Bab*$^{-}$/*Dsx*$^{+}$) cluster as the population of spatulate scale cells, and the *Scale 3* (*Bab*$^{-}$/*Dsx*$^{-}$) as the UVI scale cell precursors.

In addition, a total of 1,024 genes are differentially expressed between the two *Bab*$^{-}$ clusters (**Data 3 at** https://osf.io/yjvkc/), suggesting that while they share the property of being male-specific, UVI and spatulate scale precursors deploy distinct gene expression programs at the 40% pupal stage. For example, the spatulate *Scale2* cells are enriched for the *ivory* lncRNA gene and *yellow-c* (Fig 8A′), two markers of melanic scales in nymphalids [84–87], and express *fz3* and *vestigial*, which mark the periphery of the wing [88,89]. *ImpL2* is the ortholog of *BmIMP*, a gene required for the male-specific

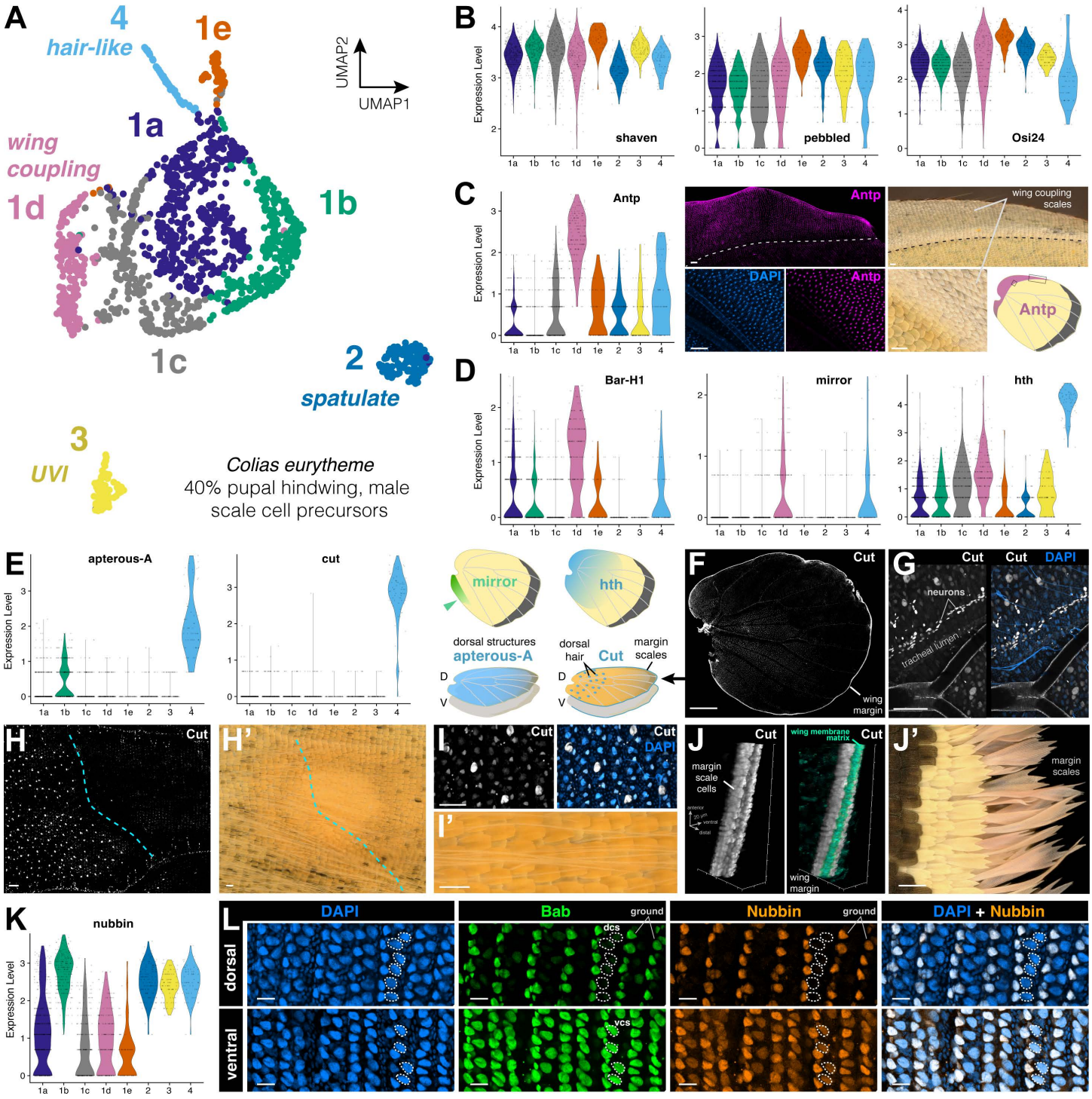


**Fig 7. Diverging gene expression profiles of male scale cell precursors at 40% development. A.** UMAP plot representing the 8 sub-clusters of scale cell precursors across a total of 1,550 cells. **B.** Violin plots for scale markers (*sv*, *peb, Osi24*) and developmental factors showing differential expression patterns across scale subtype (see text) markers (all scales). **C.** Violin plot of *Antp* expression showing enrichment in *Scale1d*, and Antp immunofluorescence (Antp 4C3 antigen) localization to unpigmented wing coupling scales [81]. **D.** Violin plots for the unpigmented scales marker Bar-H1 [25], far-posterior region marker *mirror* [82], and proximal region marker *homothorax* [80]. **E.** Violin plots for *Scale4* marker genes Cut, previously localized to large wing nuclei and wing margin [36,83], and *apterous-A*, a marker of dorsal-specific structures [79]. **F.** Immunofluorescent localization of the

Cut 2B10 antigen (gray) shows bright marking of the wing margin, and nuclear signal interspersed in the wing epithelium and in tracheal lumen. **G.** Cut signal in tracheal lumen likely corresponds to chains of differentiating neurons. **H–I′.** Large nuclei with Cut signal likely correspond for dorsal wing hair, restricted to the proximal side of the discal crossvein (dotted line). **J–J′.** Expression of Cut in wing margin scales likely corresponds to the precursors of elongated margin scales. Cyan: staining of the basal wing membrane, here shown using the non-specific signal from animmunofluorescence assay using a guinea pig polyclonal anti-Dve antibody. K. Violin plot of *nubbin* expression. **L.** Antigenicity of Nubbin 2D4 revealing repression of Nubbin in dorsal scale cells (dcs) and lower signal in ventral scale cells (vcs). Scale bars: Scale bars: C, G, H, H′, I′, J′ = 100 μm; F = 1 mm; I, L = 20 μm. Feature count matrices and Seurat objects used for the generation of Fig 7A–7E, 7K are available at the Open Science Framework Repository [78].

https://doi.org/10.1371/journal.pbio.3003233.g007

splicing of *Dsx* in *Bombyx* [90], and is restricted to the *Dsx*⁺ spatulate *Scale2* cells here, suggesting it may play a similar role in butterflies.

### ChIP-seq profiling of Bab genome-wide occupancy identifies potential gene targets

Single-cell analyses revealed the two populations of male-specific scale types are the most divergent, implying that a specific gene expression program specifies their morphology. Of particular interest, Bab may be a repressor of a network of genes involved in specifying the specialized ultrastructures that mediate UV-iridescence. To further explore what genes contribute to this ultrastructural specialization, we used ChIP-seq to profile Bab genome-wide occupancy, using fixed nuclei from *C. eurytheme* wings sampled at the 40% and 60% stages, with two biological replicates per stage (Fig 9A, 9B**, Data 4 at** https://osf.io/yjvkc/). Following MEME-ChIP motif discovery, the imputed Bab binding matrix recovered the AT-rich sequence profile previously established for *Drosophila* Bab1 using DNAse footprinting assays [91], validating the specificity of our ChIP-seq assay. The intersection of predicted Bab occupancy sites at the two stages results in a list of 1,482 candidate genes with at least one stable Bab-binding site in their intragenic interval or immediately adjacent intergenic regions (Fig 9C). Among these, 77 genes are upregulated and 53 are downregulated in the Bab⁻ clusters *Scale2*/*3* relative to Bab⁺ clusters, thus forming a stringent list of candidate transcriptional targets for Bab (**Data 5 at** https://osf.io/yjvkc/). It is unclear if Bab, a BTB-domain transcription factor, acts solely as a transcriptional repressor, or if it can also act as a co-transcriptional activator [91–93]. It thus remains uncertain whether the transcriptional targets of Bab should correlate positively or negatively with *Bab* expression, and we illustrate both possibilities with genes that present Bab binding sites and are either enriched or repressed in clusters *Scale2* and *Scale3*.

For example, the *Bab* locus itself shows multiple Bab ChIP peaks, suggesting it may be auto-regulated by negative and positive feedbacks (Fig 9D). The *Dsx* locus also contains multiple Bab-binding sites (Fig 9E), suggesting that Bab may be an upstream regulator of *Dsx*. Conversely, Dsx is an upstream regulator of *Bab* in flies [18,20] and also binds a putative intronic enhancer of *Bab* in swallowtail butterflies [94]. Our data thus suggests that *Dsx* and *Bab* cross-regulate each other, resulting in feedback that may enforce complex dynamics and switches in their expression during sexual differentiation. The transcription factor genes *Msx1* (*Msh*/*Drop* ortholog in *D. melanogaster*), and *Msx2* are organized in tandem in butterflies, similarly to *Tribolium* [95], and show multiple Bab-binding sites. *Msx2* is a top marker of *Scale3*, while *Msx1* marks both *Bab*– clusters *Scale2-3*, suggesting Bab may act as a repressor at this locus. Thus, not only does Bab provide regulatory feedback on itself and *Dsx*, it may also regulate other transcription factors, and these findings suggest that the gene regulatory networks that determine scale identity could be more complex than previously appreciated.

Another class of genes appearing as UVI-regulating candidates is the conserved family of Obstructor-secreted proteins, which play roles in chitin modifications and cuticle properties [96–98]. We found that the five members of this family are clustered in tandem in *C. eurytheme*, and that while *Obst-A* and *Obst-E* are not detected in scale cells, *Obst-B*, *Obst-C* (*gasp*) and *Obst-D* (*Peritrophin-A*) are all consistently expressed as markers of the UVI cell cluster *Scale3* (Fig 9H–9I″). Strikingly, the promoter regions of these three genes show strong Bab ChIP-seq signals, suggesting Bab may repress the expression of *Obstructor* family genes. Similarly, the chitin deacetylase genes *Vermiform* and *Serpentine* occur in tandem, show evidence of Bab-binding, and are enriched in the spatulate scale cluster *Scale2* (Fig 9J–9K′).

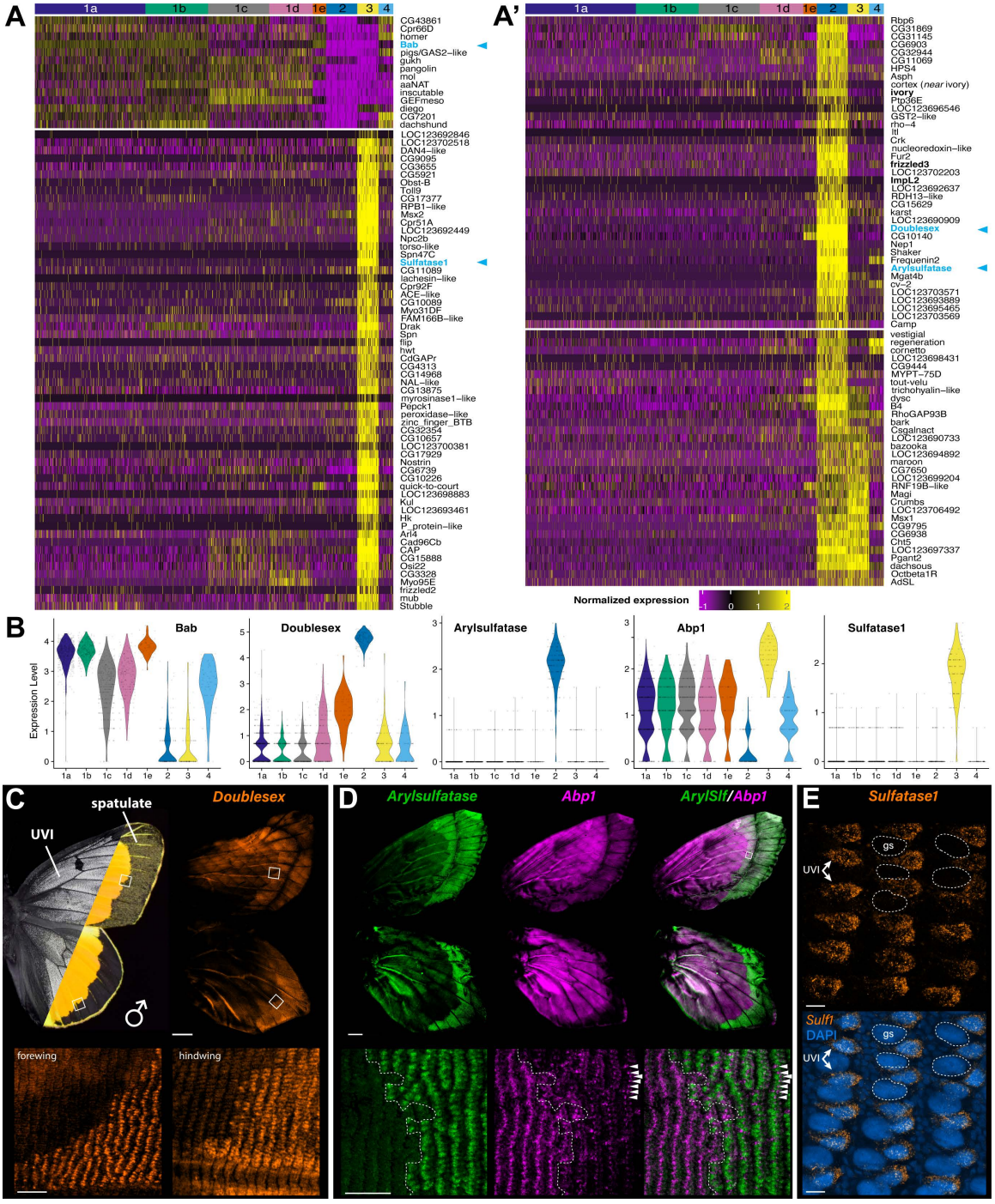


**Fig 8. Transcriptional divergence of UVI and spatulate scale cell precursors.** All experiments correspond to male wing tissues at 40% pupal development. **A–A′.** Heatmap plot of the 145 most-significant differentially expressed genes in clusters *Scale2* and *Scale3* relative to the remaining scale cell clusters (**Data 2-3 at** https://osf.io/yjvkc/). The top-left panel (A) shows genes downregulated in *Scale2* and *Scale3*. The remaining panels (A–A′) show genes that are enriched in either or both of these clusters. Bold: see text for details. Blue: see panels C–E for spatial expression. **B.** Violin plots for *Bab* and marker genes used for the spatial identification of the *Scale2* and Scale*3* cluster. **C.** HCR localization of *Dsx* mRNA (exons 1-2) in male dorsal wings. **D.** HCR localization of *Arylsulfatase* (green) and *Abp1* (magenta), respectively, tested as positive and negative markers of the *Scale2* cluster, in male dorsal wings. *Arylsulfatase* is found in the dorsal cover scales of the male marginal region. Arrowheads: ground scale expression of *Abp1* in the marginal region, without overlap with *Arylsulfatase.* **E.** HCR localization of *Sulfatase1* mRNA, tested as a marker of the *Scale3* cluster, in the medial

region of a male dorsal hindwing. Expression is restricted to alternating scale precursor cells corresponding to the presumptive UVI scales, while ground scale precursor cells (gs; dotted lines) are negative. Scale bars: C-D (top) = 1 mm; C, D insets (bottom) = 100 μm; E = 10 μm. Feature count matrices and Seurat objects used for the generation of Fig 8A, 8B are available at the Open Science Framework Repository [78].

https://doi.org/10.1371/journal.pbio.3003233.g008

Overall, these data sketch a broad overview of the potential targets of Bab at both the 40% and 60% stages, leveraging differential expression from both *Bab*⁻ cells types—the spatulate and UVI scale cell precursors. Presently, we do not have functional evidence that low *Bab* expression in *Scale2* cells is required for spatulate scale specification. In contrast, loss-of-function assays and heterozygous phenotypes of Bab alleles show it is necessary and likely sufficient for UVI scale repression [29]. We thus sought to further refine the set of potential regulatory targets of Bab by focusing on genes that are differentially expressed in the *Scale3* UVI cells (UVI-DE). Interestingly, genes with Bab ChIP signals are significantly more likely to be UVI-DE (Fig 10A). Stringent filtering criteria result in a list of 87 UVI-DE genes with 3 or more Bab ChIP binding peaks (**Data 6 at** https://osf.io/yjvkc/). Within this set, 17 genes have known functions in *Drosophila* that relate to cytoskeletal dynamics or cuticle formation (Fig 10B, 10C), two key processes that we expect to regulate ridge spacing and multilayering. For example, the loci encoding the nuclear hormone receptor Eip75b and cytoskeletal regulator Multiple wing hair (Mwh) each show more than 50 Bab ChIP sites, and are upregulated in UVI scale precursors, suggesting that Bab directly acts as a transcriptional repressor at these genes.

### Differentially expressed genes experiencing selective sweeps

*C. eurytheme* hybridizes in sympatry with its UV-negative sister species *C. philodice* in the Eastern US [29]. We reasoned that key downstream loci in the formation of UVI scales could also show signals of selection that are present in *C. eurytheme* but absent in *C. philodice.* Selective sweeps were calculated as the μ statistic in RAiSD [99] and intervals called with *bedtools*, taking a threshold of the top 1% of μ values. 449 sweeps were detected in total, and 63 were found only in *C. eurytheme*. Of 11,647 unique ChIP binding sites, just 29 were found to be within selective sweeps, and of these, 4 are private to *C. eurytheme*, one is private to *C. philodice*, and 24 have undergone a sweep in both species (**Data 7 at** https://osf.io/yjvkc/). Notably *Stubble (Sb),* a determinant of bristle actin bundle number in flies [100,101], has two ChIP peaks that have undergone a sweep in *C. eurytheme* and not *C. philodice*. Most sweeps do not directly intersect ChIP binding sites, but 313 sweeps near 287 genes are in proximity to both ChIP binding sites and selective sweeps, including 58 UVI-DE genes (Fig 10D, **Data 8 at** https://osf.io/yjvkc/). Notably, *Mwh*, *Sb*, *Bab,* and ABCG20 (Fig 10B) all have private sweeps in *C. eurytheme*, along with *pdm3*, a gene known to be involved in patterning and pigmentation in other butterflies [33], and SCAR, an Arp2/3 interacting protein involved in bristle intracellular patterning in flies [102]. The combination of differential expression, binding by Bab, and signals of selection on this subset of UVI scale-expressed genes provide an initial glance at the candidate genes that fine-tune the specialized ultrastructure of UVI scales.

## Discussion

In this study, we tied scale sexual dimorphism to context-dependent functions of Dsx, and identified two male-specific scale types that are demonstrably regulated by the expression of DsxF and Bab (the UVI scales), or by DsxM/F (the spatulate scales). Then we delved into the single-cell transcriptomics of the male wing tissue and recovered the developmental precursor cell populations of these two derived scale types, providing new insights on how cell-autonomous sexual identity is leading into specialized ultrastructures.

### Antagonistic roles of Dsx isoforms in marginal wing patterning

CRISPR and RNAi phenotypes resulted in concordant phenotypes, and highlight the versatility of Dsx in mediating the sexually dimorphic differentiation of UVI and spatulate scale types, as well as the patterning of marginal melanic bands that are proper to each sex (Fig 5A, 5F).

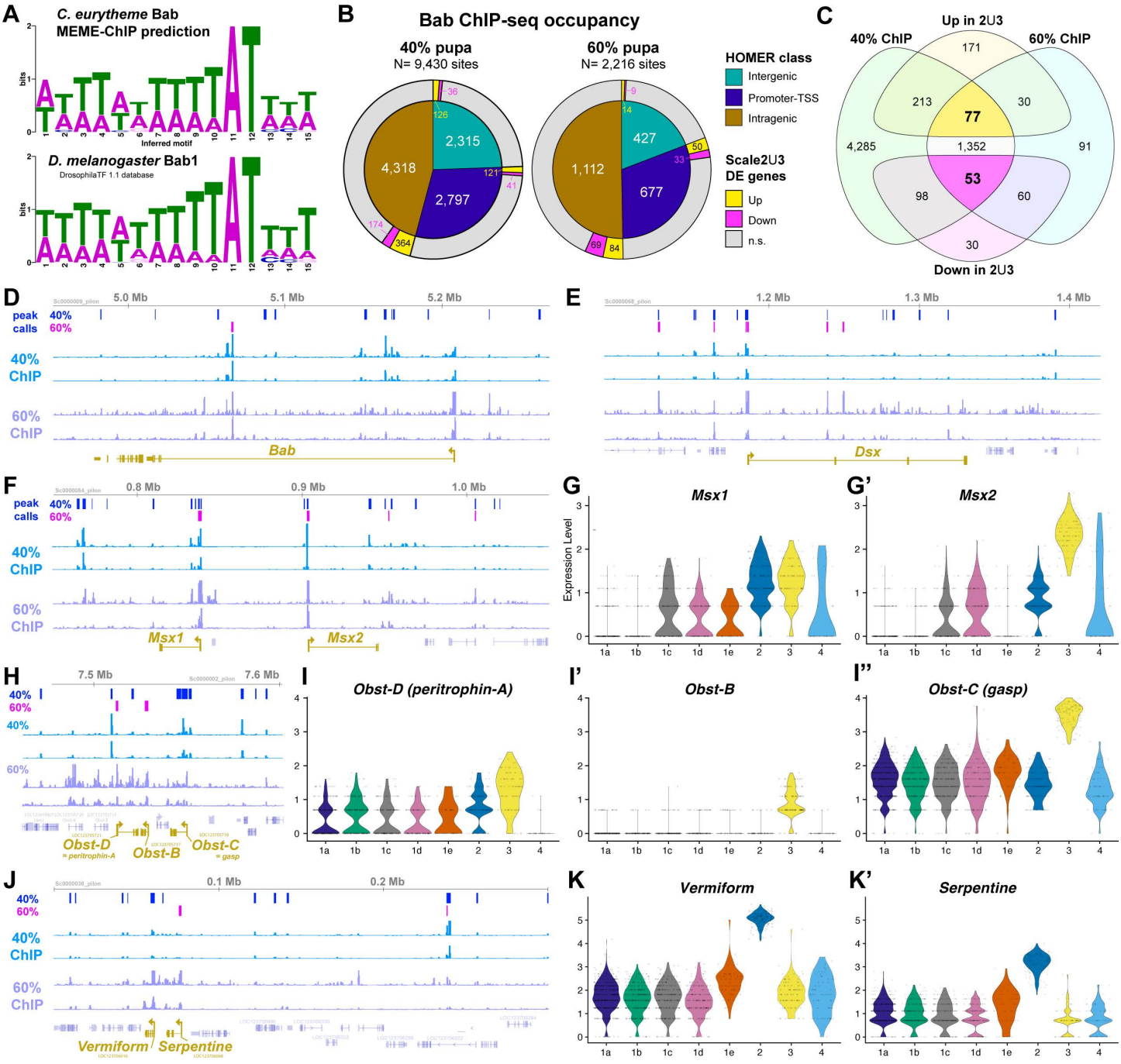


**Fig 9. ChIP-seq profiling of Bab identifies potential target genes involved in the differentiation of Bab– scale types. A.** MEME-ChIP predicted motif for Bab occupancy as inferred from the Bab ChIP pupal wing dataset (top), resembling a previous binding profile for a Bab fly ohnologue (bottom). **B.** Summary of the position of all predicted Bab ChIP-seq binding sites across two datasets, at the 40% and 60% pupal stages **(Data 4-5 at** https://osf.io/yjvkc/). Inner circles: HOMER classification of imputed binding sites relative to gene annotation features. Outer rings: overlap with genes that are among the differentially expressed (DE) genes in *Scale2* (spatulate) and/or *Scale3* (UVI) relative to other scale types. C. Venn diagram featuring the numbers of genes identified as Bab-bound and differentially expressed (DE) in the *Scale2-3* clusters, resulting in an intersection of 77 (up) and 53 (down) DE genes with binding sites identified across two stages. **D, E, F, H, J.** Genomic intervals featuring the Bab ChIP-seq profiles across replicates and peak calls at each stage, including at the promoters of *Scale2-3* markers (bottom, buff color). **G–G′, I–I″, K-K′.** Violin plots of snRNAseq scale cluster expression for the same marker genes.

https://doi.org/10.1371/journal.pbio.3003233.g009

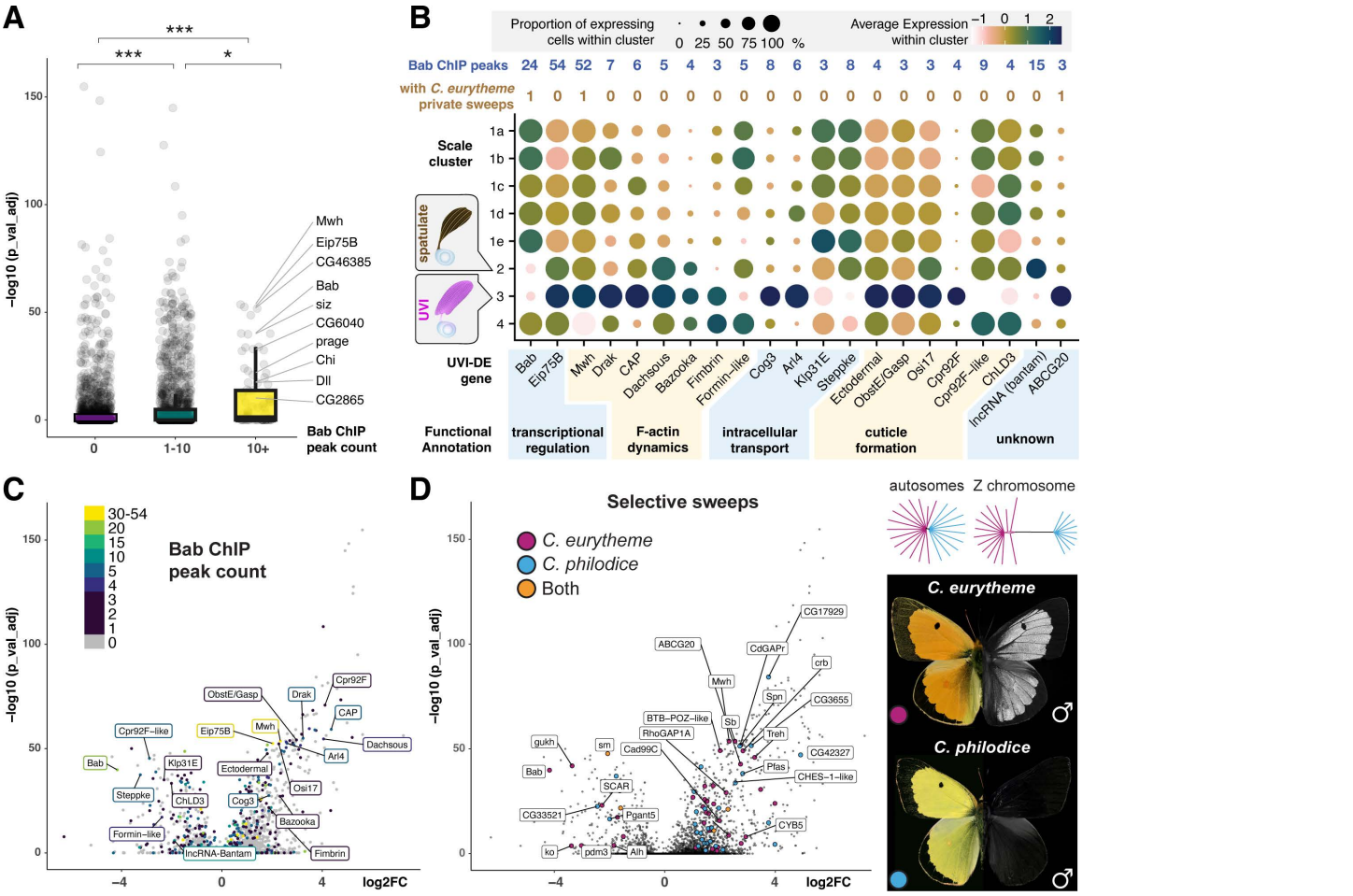


**Fig 10. Potential targets of Bab regulation in the UVI scale type.** A. Box and whiskers plot of probability of differential expression, binned by number of called Bab ChIP sites in proximity to each gene (Wilcoxon rank sum tests; *: $p<0.01$; ***: $p<1e{-}15$). B. Expression dot plot visualization of selected UVI-DE genes ($log2FC>1.8$, adjusted $p<0.01$) with at least 3 Bab ChIP peaks and potential roles in ultrastructural specialization **(Data 5 at** https://osf.io/yjvkc/). **C, D.** Volcano plots of UVI-DE genes **(Data 7-8 at** https://osf.io/yjvkc/), colored by number of Bab ChIP sites (C), and by the presence of selective sweeps in a sympatric population of *C. eurytheme* x *C. philodice* (D). These two morphospecies hybridize and show genome-wide admixture across autosomes (dendrograms reproduced from [29], resulting in a population polymorphic for UV iridescence (present in *C. eurytheme*, absent in *C. philodice*).

https://doi.org/10.1371/journal.pbio.3003233.g010

As *Dsx* mosaic knock-outs yielded clonal effects with sharp boundaries for these traits, we inferred that Dsx had cell autonomous effects on the control of UVI and spatulate scale cell identities. In contrast, marginal patterning did not show such clonal effects, which could have consisted in splitting effects on the female-like yellow spots, abrupt discontinuities in the position of the orange/black pattern boundary, or in sharp UVI-negative clones in the distal region in males. We propose that this is because Dsx isoforms influence the masculinization or feminization of these marginal patterns in a non-autonomous manner, probably by controlling extracellular signaling and morphogenetic processes that take place in early pupal stages. This dual regulation would be consistent with current models suggesting that DsxF and DsxM isoforms target an identical set of genes, but confer opposite effects on gene expression [18,19]. The Wnt signaling pathway, the transcription factors Spalt and Distal-less, and the melanic scale determinant *ivory*/*miR193* have been implicated the patterning of pierid marginal bands [87,103–107], and could thus be targets of differential regulation by Dsx isoforms.

Likewise, we found that DsxM and DsxF, respectively, masculinize and feminize the state of marginal dorsal cover scales, by promoting or repressing the differentiation of male-specific spatulate scales. Surprisingly, *Dsx* mKOs induced reciprocal transformations in both directions (Fig 4B, 4C), implying that the canonical-spatulate states are switchable in each sex and under antagonistic regulation from Dsx (Fig 5A). To explain this, we speculate that DsxM and DsxF have opposite effects on the expression of the same target genes—a model that accounts for some of the mode of action of Dsx in other insects [108,109]. In future studies of *Colias* wing dimorphism, it will be interesting to compare the single-nucleus transcriptomes of both male and female tissues, and to establish the occupancy profile of Dsx in each sex [94].

### UV dichromatism is DsxM-independent but requires DsxF-mediated activation of Bab

Bab is required to prevent UV-iridescence in most scales, and is repressed in the orange dorsal cover scales of male *C. eurytheme*, thus allowing UV-iridescence in a small subset of scales [29]. Previous work on *Drosophila* sexual dimorphic traits such as the pigmented abdomen, sex combs, and gonadal stem nich, collectively suggest that DsxF and DsxM have an activating and repressing effect on *Bab*, respectively [20,21,110,111]. Our experiments rule out a repressing role of DsxM on Bab because Dsx perturbation did not induce loss of UV-iridescence in males. In addition, snRNAseq, HCR mRNA detection assays, and immunofluorescence did not detect *DsxM* in the UVI cell precursors, *i.e.,* the male dorsal cover scales of the medial region. Of note, while we observed a marginal reduction in the UVI field in the vicinity of the peripheral patterns, we extrapolate that this was due to a change in the identity of the marginal patterns rather than a direct effect of DsxM on *Bab*.

In the medial region, DsxF acts as a likely transcriptional activator that maintains *Bab* expression at the 40% stage, thus repressing UVI fate. Such regulatory linkage between *Dsx* and *Bab* is reminiscent of studies of *D. melanogaster*, where DsxF activates *Bab* expression, thereby controlling the sexual dimorphism of abdominal pigmentation [20,111]. At the moment, while these data in distant insect lineages suggest that dimorphic *Bab* expression often drives sexual differentiation in a variety of tissues, it is unclear if this Dsx inputs on *Bab* regulation evolved repeatedly or if they derived from ancient, conserved interactions. Interestingly, DsxF binds an intronic *cis*-regulatory element of *Bab* during the pupal wing development of *Papilio alphenor* butterflies [94], but it remains to be determined whether this mode of regulation of *Bab* is conserved and homologous with *C. eurytheme*.

### The evolution of scale sexual dimorphisms in *Colias*

Sexually dichromatic butterflies show a general trend where female wings are usually less colorful than the male ones [112], except when colors have an aposematic function. Accordingly, UV-iridescence in pierid butterflies is either male-specific (*e.g.,* in *C. eurytheme*), or when it is found in females, it is in a much reduced or residual state than in males [29,113]. In other words, sexual differences in UVI likely involved the recruitment of an off-switch in females, rather than an on-switch in males. This is consistent with a two-step model for the evolution of UVI sexual dichromatism in pierids. First, UVI likely originated in both sexes, and this required a loss of Bab expression in the dorsal cover scales of the medial region. Later, reduction of UVI patches evolved in females by recruiting *Dsx* in the dorsal cover scales, re-activating the expression of *Bab*. This off-switch mechanism went a further step in *Zerene cesonia*, a close relative of *Colias*, where a duplicated copy of *Dsx* evolved a truncated female-specific transcript that is highly expressed in the female dorsal scales, in a pattern consistent with UVI-repression [114]. We thus postulate that *Dsx* did not contribute to the origin of the UVI scale type itself, but that its female-specific products were recruited to re-activate Bab in dorsal cover scales and thereby reduce the size of the UVI patch in females. Crucially, this model is consistent with phylogenetic models that place the origin of UVI scales in an early ancestor of Pieridae, followed by secondary reduction of UVI patterns [23].

How does this mechanism fit more broadly into evolutionary thinking? In a decade-long debate about the causes of sexual dichromatism (primarily in birds and butterflies), Arthur Wallace invoked the importance of natural selection to decrease conspicuous traits in females, while Charles Darwin favored the supremacy of sexual selection [115]. Because

males and females are often subject to different selective pressures, it is commonly accepted that the two explanations are not mutually exclusive [116,117]. In our evolutionary model, sexual selection remains a key force to explain the origin of UVI and its persistence in males [27,118], as defended by Darwin, while the spatial reduction of this trait in females supports a role for natural selection as championed by Wallace. For example, passerine birds that predate *Colias* butterflies express UV-sensitive opsins [119], and are likely to perceive male wing strokes as bright flashes of UV-color [22,31], which produce chromatic contrast on green vegetation backgrounds with low UV-emissivity (S7 Fig). Evolutionary losses and reductions of female UVI patterns may thus be linked to predator avoidance, and the recruitment of DsxF in UVI scale repression provides a possible mechanism for this sex-limited effect.

### Using snRNAseq to explore wing cell type diversity

The enormous diversity of butterfly wing patterns largely amounts to the ability of these organisms to differentiate various scale types that vary in coloration, and to organize them in space during development. Scales emerge from a single-scale cell precursor during development, and we expect that single-cell approaches to scale differentiation will uncover new insights into how tissues organize complex spatial patterns during development and how new traits evolve. In this study, single-nucleus transcriptomics allowed the detailed profiling of nearly 3,000 cells, about half of which were scale cell precursors. The snRNAseq sample consisted of a single hindwing dissected from a male *C. eurytheme* pupa, and the pooling of several individuals is unnecessary with this technique and tissue. Subsetting the initial clustering to select for scale clusters, characterized by *sv* expression [36,37], enables the detailed analysis of scale cell precursor transcriptomes in ways that have not been possible with bulk RNAseq methods (*e.g.,* for mining of top marker genes from differentiated clusters), and generated new hypotheses regarding cell type specification and specialization. Importantly, this study provides only a snapshot of gene expression profiles in a single individual and sex. Future studies of *Colias* pupal wing development could compare sexes and may benefit from analyzing tissues sampled across a tight developmental series, in order to reveal expression trajectories of differentiating cell populations.

### Transcriptomic insights on the differentiation of specialized scale ultrastructures

We found that two scale clusters lack *Bab* expression, and correspond to male-specific, Dsx-dependent scale types – the UVI and spatulate scales. Each of these types show ultrastructures that diverge from canonical scale types, with extreme variations in the spacing of longitudinal ridges (Fig 1D), and the remarkable multilayering of the UVI scale upper lamellae (Fig 1J) that yields their structural coloration [44,120].

Previous studies have shown that condensed actin filaments pre-pattern the density of ridges in butterfly scales, and then template the formation of iridescent elaborations [39,121–123]. Genes that are differentially expressed in the UVI scales provide a wealth of candidate modulators of actin dynamics including *shavenoid*, *Abp1*, *singed* (Fig 6H′), which are known to modulate actin assembly and ridge patterning in *Drosophila* bristles [102,124,125]. We found strong evidence of Bab occupancy at the UVI scale marker genes *fimbrin* and *mwh,* two key determinants of actin bundling and bristle morphology in flies, indicating they are direct targets of Bab repression (Fig 10B). Similarly, we suggest that Bab-bound DE genes with annotated functions in vesicular trafficking and cuticle formation—such as *Osi17*, *Cpr92F*, and the chitin deacetylase *ChLD3* [75,126,127]—may be direct targets of Bab regulation that participate in the sculpting of the nanostructures on the scale upper surface, including the stacking of UVI ridge lamellae. This is further strengthened by the fact that a number of these genes also show evidence of selection specifically in *C. eurytheme* and not its UV-negative sister species *C. philodice* (Fig 10D), implying either that regulatory connections are being maintained by purifying selection or that network interactions permissive for UVI scale specialization are under positive selection. While the function of these potential effectors will require further investigation, the application of snRNAseq to mid-pupal stages of butterfly wing development promises to be an exciting avenue of research for understanding how complex exoskeletal ultrastructures form and diversify.

## Methods

### Butterflies

*C. eurytheme* females were collected from an organic alfalfa field (Buckeystown, MD), and left in small cylinder cages with alfalfa for oviposition. Eggs were collected manually, washed 1′ with Benzalkonium Chloride 5%, rinsed and dried, left to hatch at 25 °C, 60% humidity, 14:10 h day:light cycle and fed with Black Cutworm artificial diet (Frontier Agricultural Sciences) supplemented with dry alfalfa powder, before transfer to Lana woollypod vetch (*Vicia villosa*) in a greenhouse environment [26]. Fifth-instar wandering larvae were moved to a growth chamber set at 28 °C, 60% humidity, 16:8 h day:light cycle, and their time of pupation recorded. Developmental times are reported as percentages, relative to a mean development time 138 h from pupation to adult emergence at 28 °C, or 170 h at 25 °C.

### CRISPR mosaic knock-outs

Eggs were collected on alfalfa shoots and leaves, washed, dried, and placed upward on thin strips of double-sided tape, on the inner side of a 1.25 oz. cup lid, and micro-injected following previously reported procedures [26,29] with an equimolar mixture of Cas9-2xNLS:sgRNA at 500:250 ng/μL. Embryos were left to hatch in cups containing vetch sprouts, and transferred to vetch sprout mats in a greenhouse environment for larval growth.

### RNAi electroporation

Dicer-substrate siRNAs (DsiRNAs) were designed against target gene exons (S2 Table), ordered at the 2 nmol scales as Custom DsiRNAs with standard purification (IDT DNA Technologies), resuspended at 100 μM in 1× *Bombyx* injection buffer (pH 7.2, 0.5 mM $NaH_2PO_4$, 0.5 mM $Na_2HPO_4$, 5 mM KCl), and stored as frozen aliquots at −70 °C until use. Electroporation procedures followed a previously described procedure [89,128]. To target the dorsal surface of male wing pupae, the negative electrode was placed in contact with the droplet of saline positioned on the ventral side of the peeled wing, while the positive electrode was in contact with the agarose pad on the dorsal side of the wing, before electroporation with 5 square pulses of 280 ms at 8 V, separated by 100 ms intervals.

### Genome annotation

The genome annotation available for *Colias croceus* (NCBI:PRJEB42949), was mapped to the best available *C. eurytheme* assembly (NCBI:GCA_907164685.1) using *Liftoff* [24,129,130]. A total of 12,908 genes had annotations transferred from *C. crocea* and 7,418 genes were obtained on reciprocal Blast against Flybase protIDs using *-blastx* with *-evalue 1e−50*, retaining best hits against subjects.

### Live nuclei preparation for single-nucleus transcriptomics

We isolated live nuclei using dounce homogenizers following previously published protocols [37,131]. Briefly, a hindwing was dissected from a single male individual (53 h old pupa at 28 °C, 40% stage) in cold 1× phosphate-buffered saline (PBS) and immediately transferred for sequential douncing in homogenization buffer (250 mM sucrose, 10 μM Tris pH 8.0, 25 mM KCl, 5 mM $MgCl_2$, 0.1% Triton-X 100, 0.2 U/μL RNasin Plus, 1× Protease Inhibitor, 0.1 mM Dithiothreitol). The homogenized tissue was transferred to a new 1.5 mL tube and spun down in a fixed-rotor centrifuge at 4 °C for 10 min at 1,000*g*, before resuspending in 500 μL nuclei suspension buffer (PBS, 1% Bovine Serum Albumin, 0.2 U/μL RNasin Plus). The nuclei suspension was filtered using a 40-μm PluriSelect filter and 10 μL were drawn for staining with trypan Blue. Nuclei quality was assessed based on membrane integrity and nuclei were counted using a hemocytometer, yielding a concentration within the target range of 600–900 nuclei/μL. Nuclei suspension was processed for cDNA library preparation with a target output of 3,000 nuclei per sample.

### snRNAseq library preparation and sequencing

The droplet-based 10× Genomics Chromium Next GEM Single Cell 3′ Reagent Kit v3.1 with Dual Indexes was used to prepare multiplexed cDNA libraries from nuclei suspensions [37]. Libraries were pooled for PE150 sequencing on a Novaseq S2 flow cell at a target depth of 200,000 reads/nucleus. Raw reads are accessible at the NCBI SRA (NCBI:SRS12272185).

### snRNAseq data preprocessing and analysis

BCL files were demultiplexed into *fastq* files using *bcl2fastq*. Raw and filtered CellRanger-generated count matrices with the flag *--include-introns* were used for downstream analysis and are available in an online data repository [78]. Seurat v5.0 was used for preprocessing of Seurat objects, first filtered to remove low-quality Gel Beads-in-emulsion (GEMs) with *nCounts* < 300, *nFeatures* < 3,000 and *percent.mt* > 3%. Library sizes, number of per-cell features and proportion of reads mapped to mitochondrial genome were used as quality control metrics. The sample at 40% pupal development was normalized using SCTransform with an additional regression of nuclei based on percentage of mitochondrial reads (*vars.to.regress* = "*percent.mt*"), before performing *RunPCA* and *RunUMAP* using top 20 PCs, after which *FindNeighbors* and *FindClusters* functions were invoked to generate 2D layouts of graph-based clusters. Clustering resolution of 0.1 was used after examining cluster stability using *R*/*clustree* on clustering resolutions at 0.1, 0.2, 0.5, 0.7, and 1.0.

For cluster annotation of recovered nuclei from the 40% sample, we identified differentially expressed genes using *FindAllMarkers* in Seurat (Wilcoxon Rank Sum test with Bonferroni correction for multiple testing; adjusted $p < 0.05$). Marker genes were identified based on genes detected in a minimum of 25% of the cells within the cluster and a *log2FC* > 0.25 between the cells in the cluster and all remaining cells. Focusing on scale-building nuclei, the whole object was subset for *shaven*-expressing nuclei. Preprocessing steps were performed as previously mentioned but using 0.2 resolution for *FindClusters*. Heatmap was generated using *R*/*ComplexHeatmap* [132,133] and genes were ordered via unsupervised hierarchical clustering of 4 k-means groups.

Following cluster identification, we subset the whole object for scale clusters *Scale1-4* using expression of canonical markers *sv* and *ss*. Normalization with *SCTransform* was performed on the original, filtered count matrix as mentioned previously, following *RunPCA* and *RunUMAP* with top 10 PCs, before *FindNeighbors* and *FindClusters* were performed with a clustering resolution of 0.1. *FindMarkers* comparing each cluster of interest with the rest of the subsetted object adjusted $p < 0.05$, *log2FC* > 1.25, *min.pct* = 0.25) was used to identify marker genes.

### Preprocessing and analysis of Chromatin-Immunoprecipitation (ChIP)-sequenced data

ChIP-seq libraries were prepared from live pupal wings (S1 Text), and sequenced as PE42 reads for samples at 40% and PE37 reads for samples at 60%, available on the NCBI SRA, PRJNA1148116). The *C. eurytheme* genome was indexed using *bowtie2* (2.5.3). *FastQC* was used to assess the quality of fastq files. Trimmed reads were aligned to the genome using *bowtie2* (2.5.3), sorted using *samtools* (1.15.1), filtered, and *MarkDuplicates* using *picard tools* (2.26.8) from GATK (4.2.4.0) was invoked to remove duplicate reads. Filtered and uniquely mapping reads were used for peak calling using MACS3, with options *q* = *0.01*, BAMPE, and an effective genome size of 328,651,476 bp. Relaxed peak calling with a *p* = *0.05* threshold was performed, followed by further statistical correction using the Irreproducible Discovery Rate framework (version 2.0.4.2), which assessed the reproducibility of called peaks between the two replicates based on a fraction of false positive peaks [134,135]. This generated a final list of peaks for each time point at the maximum False Discovery Rate of 0.05 (Data 4 at https://osf.io/yjvkc/). Peak annotation was performed using HOMERv4 *annotatePeaks.pl*, to assign each peak to a genomic region of a nearby gene [136]. For visualization in IGV, the *deeptools* (3.5.4) function *bamCompare* was used to subtract input *bam* files from each corresponding replicate and derive *bigWig* files for each sample [137]. To identify conserved motifs within peaks across four samples, *fasta* files for peak intervals were extracted from

IDR output using *bedtools* (2.28.0) function *getfasta*, and served as the input for motif discovery using the Combined Fly reference set in MEMECHIP [138]. Finally, gene lists from Data 2 and Data 4 were merged to identify candidate genes regulated by Bab, with differential expression in the $Bab^{-}$ scale clusters and Bab-binding ChIP peaks present in both pupal stages, 40% and 60% development.

### Immunohistochemistry and confocal imaging

Antibody stainings were performed as previously described [29]. In short, pupal wings were dissected in cold PBS and fixed in fixative (4% methanol-free paraformaldehyde diluted in PBS, 2 mM egtazic acid) at room temperature for 13−20 min, washed four times in PT (PBS, 0.1% Triton-X 100), blocked in PT-BSA (PT, 0.5% Bovine Serum Albumin), incubated overnight at 4 °C with primary antibody dilutions in PT-BSA, washed in PT, incubated 2 h with secondary antibody dilutions in PT-BSA (1:500 dilutions, following two short centrifugation steps to pellet down particules before incubation with the wings), washed in PT, incubated in 50% glycerol with with 1 μg/mL DAPI (4′,6-diamidino-2-phenylindole), mounted on glass slides with 70% glycerol or SlowFade Gold mountant under a #1.5 thickness coverslip, and sealed with nail varnish before confocal imaging. Antibodies used in this study were a polyclonal, affinity purified anti-*Colias* Bab [29] rabbit antibody (1:100 dilution); several monoclonal mouse antisera (1:50–1:100; Developmental Studies Hybridoma Bank) targeting DsxDBD [57], Nubbin [139], Cut [140], and Antp [141]; and a polyclonal, affinity purified anti-Dve [142] guinea pig antibody (1:400; kind gift of Mike Perry). Secondary antibodies included conjugated AlexaFluor488 anti-Mouse IgG (Life Technologies, CA) at 1:500 dilution, conjugated AlexaFluor647 anti-Rabbit IgG (Life Technologies, CA) at 1:500 dilution, and conjugated AlexaFluor555 goat anti-guinea pig IgG (Abcam, UK). Stacked acquisitions were obtained on an Olympus FV1200 confocal microscope mounted with PLANAPO 20× and 60× objectives. Immunofluorescent stains of whole pupal wings were imaged with a Zeiss Cell Observer Spinning Disk confocal microscope mounted with a 10× objective (Plan-Apochromat, 0.45 NA) for HCR mRNA stainings, or with an Olympus BX53 epifluorescent microscope mounted with an UPLFLN 4× objective. Stitching correction was performed on spinning disk confocal-acquired stitches using the ZEN software.

### Detection of selective sweeps

An admixed population of *C. eurytheme* and *C. philodice* (Buckeystown, MD) was previously resequenced, genotype-called, filtered, and analyzed [29]. RAiSD was used to calculate the μ statistic separately on each of *C. eurytheme* and *C. philodice* with default parameters [99]. Swept intervals were identified by taking the top 1% of μ for each species and merging the called sites with *bedtools merge*. Each called interval was then connected to its nearest gene using *bedtools closest*, and intersected with called ChIP sites with *bedtools intersect*.

## Supporting information

**S1 Fig. Targeted mutagenesis of *Dsx* monomorphic exons in *C. eurytheme*. A.** Overview of the *Dsx* locus in the *Colias croceus* genome annotation. The gene structure is inferred from RNAseq intron-spanning reads available on the NCBI Genome Browser, and features three major isoforms. The male isoform (*DsxM*, ENSCEUT00000038409.1) spans an open-reading frame on exons 1, 2 and 5. The female isoforms (*DsxF*, ENSCEUT00000038412.1 and ENSCEUT00000038415.1) both span an open-reading frame on exons 1, 2 and 3. CRISPR sgRNA targets were designed on the matching version of the *C. eurytheme* genome (arrowheads) and predicted to impact all isoforms. The *exon 1* target overlaps with the region encoding the DM DNA binding domain of Dsx, while the *exon 2* targets corresponds to the Dsx dimerization domain. **B.** Genotyping of a mosaic crispant following the targeting of *Dsx exon2* using Synthego ICE chromatogram deconvolution. Dotted line: predicted cut site.
(TIF)

**S2 Fig. *Dsx* crispant phenotypes in *C. eurytheme* males.** *Dsx* mosaic knock-out effects are exclusively visible in the marginal section of the male dorsal wings (left panels), with a proximal extension of the melanic band, a proximal regression of the distal border of the UV iridescent region (also visible in the visible spectrum as a yellow extension), and a transformation of scent-related marginal scales into regular melanic scales (not visible here). There were no visible effects on ventral sides (right panels). Bottom rows: UV-spectrum photography (320–400 nm).
(JPG)

**S3 Fig. *Dsx* crispant phenotypes in *C. eurytheme* females.** Female *Dsx* crispants show a male-like regression of the marginal melanic band, a transformation of marginal melanic scales into male-like scent-related scales (not visible here), and widespread gains of UV-iridescence, all restricted to the dorsal side of each specimen (left panels). There were no visible effects on ventral sides (right panels). Bottom rows: UV-spectrum photography (320–400 nm).
(JPG)

**S4 Fig. Masculinization of female forewing marginal scales following DsxF mosaic knock-out.** Additional example of a *DsxF* mKO phenotype in a female dorsal forewing marginal region. The white line delineates the clonal boundary between KO (top) and WT areas. Stars demark scales with intermediate canonical-to-spatulate transformations. The dorsal margins of the female forewing show black ground scales, here transformed to a male-like yellow state in mKO areas (arrowheads). Scale bars: 50 μm.
(JPG)

**S5 Fig. DsxF expression in the dorsal cover scales of both medial and marginal regions.** Immunofluorescent detection of the Bab (green) and DsxDBD (magenta) antigens in both the cover scales (dcs) and ground scales (gs) of female wings sampled at the 30% (**A, B**) and 40% stages (**C, D**). The Dve antigen (cyan) marks ground scales. Socket cells (so) are visible at the 30% stage in the medial region only (A). Scale bars: 10 μm.
(JPG)

**S6 Fig. Quality control metrics for 40% *C. eurytheme* wing tissue snRNAseq.** These plots compare CellRanger outputs before **(A)** and after **(B)** filtering for *nCounts* > 3, *nFeatures* > 300, *percent.mt* < 4%. Left panels: number of genes detected in each cell relative to percentage mitochondrial reads within each cell. Right panels: number of genes detected in each cell relative to the total number of molecules detected within a cell. $R^2$ values indicate the coefficient of determination in each comparison.
(JPG)

**S7 Fig. Conspicuous UV-iridescence during male wing flickering and flight.** Eight consecutive video frames of a male *C. eurytheme* butterfly under natural sunlight. UV-A imaging (315–400 nm) was done using a full-spectrum converted Panasonic G3 camera, mounted with a Kyoei-Kuribayashi 35 mm F3.5 lens on a helicoid focusing adapter, and stacked Hoya U-330 and Schott BG39,1.5 mm glass filters eliminating the visible and infrared wavelengths above 400 nm. The butterfly is seen flickering its wings in the first three frames, while resting on a nectaring plant. Take-off and flight are visible on the following frames. Green vegetation is usually UV-absorbing, with the rare exception of pollinator-attracting signals such as the outer rings of *Rudbeckia hirta* flowers, as shown here. Female *C. eurytheme* are undetectable with this set-up due to their lack of iridescence.
(TIF)

**S1 Table. Summary of *Dsx* CRISPR KO injections experiments.**
(JPG)

**S2 Table. DsiRNA mixes used in electroporation experiments for gene expression knockdowns.**
(JPG)

**S1 Text. Supplementary Text.**
(PDF)

## Acknowledgments

We thank Rachel Canalichio and the staff of the Harlan W. Hilbur Greenhouse at the GWU for providing butterfly host plants; the GW Nanofabrication and Imaging Center, Patricia Hernandez and Aleksandar Jeremic for providing access to confocal microscopes; the Duke University Sequencing and Genomic Technologies Shared Resource for assistance with library sequencing; Alejandro Berrio and Carlos Arias for bioinformatics assistance; Hedgeapple Farms for providing access to field collection sites; and Brian Counterman, Vincent Ficarrotta, and Adam Porter for stimulating discussions on ultraviolet dichromatism.

## Author contributions

**Conceptualization:** Ling S. Loh, Joseph J. Hanly, Gregory A. Wray, Arnaud Martin.

**Funding acquisition:** Joseph J. Hanly, Robert D. Reed, W. Owen McMillan, Gregory A. Wray, Arnaud Martin.

**Investigation:** Ling S. Loh, Joseph J. Hanly, Alexander Carter, Martik Chatterjee, Martina Tsimba, Donya N. Shodja, Luca Livraghi, Christopher R. Day, Arnaud Martin.

**Resources:** W. Owen McMillan, Gregory A. Wray, Arnaud Martin.

**Supervision:** Ling S. Loh, Arnaud Martin.

**Writing – original draft:** Ling S. Loh, Arnaud Martin.

**Writing – review & editing:** Joseph J. Hanly.

## References

1. Blackmon H, Ross L, Bachtrog D. Sex determination, sex chromosomes, and karyotype evolution in insects. J Hered. 2017;108: 78–93. https://doi.org/10.1093/jhered/esw047
2. Saccone G. A history of the genetic and molecular identification of genes and their functions controlling insect sex determination. Insect Biochem Mol Biol. 2022;151:103873. https://doi.org/10.1016/j.ibmb.2022.103873 PMID: 36400424
3. Siddall A, Harvey-Samuel T, Chapman T, Leftwich PT. Manipulating insect sex determination pathways for genetic pest management: opportunities and challenges. Front Bioeng Biotechnol. 2022;10:867851. https://doi.org/10.3389/fbioe.2022.867851 PMID: 35837548
4. Laslo M, Just J, Angelini DR. Theme and variation in the evolution of insect sex determination. J Exp Zool B Mol Dev Evol. 2023;340(2):162–81. https://doi.org/10.1002/jez.b.23125 PMID: 35239250
5. Chikami Y, Okuno M, Toyoda A, Itoh T, Niimi T. Evolutionary history of sexual differentiation mechanism in insects. Mol Biol Evol. 2022;39(7):msac145. https://doi.org/10.1093/molbev/msac145 PMID: 35820410
6. Baral S, Arumugam G, Deshmukh R, Kunte K. Genetic architecture and sex-specific selection govern modular, male-biased evolution of double-sex. Sci Adv. 2019;5(5):eaau3753. https://doi.org/10.1126/sciadv.aau3753 PMID: 31086812
7. Verhulst EC, van de Zande L. Double nexus--Doublesex is the connecting element in sex determination. Brief Funct Genomics. 2015;14(6):396–406. https://doi.org/10.1093/bfgp/elv005 PMID: 25797692
8. Diamandi JA, Duckhorn JC, Miller KE, Weinstock M, Leone S, Murphy MR, et al. Developmental remodeling repurposes larval neurons for sexual behaviors in adult *Drosophila*. Curr Biol. 2024;34(6):1183-1193.e3. https://doi.org/10.1016/j.cub.2024.01.065 PMID: 38377996
9. Prakash A, Monteiro A. Doublesex mediates the development of sex-specific pheromone organs in bicyclus butterflies via multiple mechanisms. Mol Biol Evol. 2020;37(6):1694–707. https://doi.org/10.1093/molbev/msaa039 PMID: 32077943
10. VanKuren NW, Doellman MM, Sheikh SI, Palmer Droguett DH, Massardo D, Kronforst MR. Acute and long-term consequences of co-opted doublesex on the development of mimetic butterfly color patterns. Mol Biol Evol. 2023;40(9):msad196. https://doi.org/10.1093/molbev/msad196 PMID: 37668300
11. Camara N, Whitworth C, Dove A, Van Doren M. Doublesex controls specification and maintenance of the gonad stem cell niches in *Drosophila*. Development. 2019;146.

12. Zinna RA, Gotoh H, Kojima T, Niimi T. Recent advances in understanding the mechanisms of sexually dimorphic plasticity: insights from beetle weapons and future directions. Curr Opin Insect Sci. 2018;25:35–41. https://doi.org/10.1016/j.cois.2017.11.009 PMID: 29602360
13. Zhou C, Pan Y, Robinett CC, Meissner GW, Baker BS. Central brain neurons expressing doublesex regulate female receptivity in *Drosophila*. Neuron. 2014;83(1):149–63. https://doi.org/10.1016/j.neuron.2014.05.038 PMID: 24991959
14. Yuzawa T, Matsuoka M, Sumitani M, Aoki F, Sezutsu H, Suzuki MG. Transgenic and knockout analyses of Masculinizer and doublesex illuminated the unique functions of doublesex in germ cell sexual development of the silkworm, *Bombyx mori*. BMC Dev Biol. 2020;20(1):19. https://doi.org/10.1186/s12861-020-00224-2 PMID: 32957956
15. Nojima T, Rings A, Allen AM, Otto N, Verschut TA, Billeter J-C, et al. A sex-specific switch between visual and olfactory inputs underlies adaptive sex differences in behavior. Curr Biol. 2021;31(6):1175-1191.e6. https://doi.org/10.1016/j.cub.2020.12.047 PMID: 33508219
16. Rideout EJ, Dornan AJ, Neville MC, Eadie S, Goodwin SF. Control of sexual differentiation and behavior by the doublesex gene in *Drosophila melanogaster*. Nat Neurosci. 2010;13(4):458–66. https://doi.org/10.1038/nn.2515 PMID: 20305646
17. Robinett CC, Vaughan AG, Knapp J-M, Baker BS. Sex and the single cell. II. There is a time and place for sex. PLoS Biol. 2010;8(5):e1000365. https://doi.org/10.1371/journal.pbio.1000365 PMID: 20454565
18. Clough E, Jimenez E, Kim Y-A, Whitworth C, Neville MC, Hempel LU, et al. Sex- and tissue-specific functions of *Drosophila* doublesex transcription factor target genes. Dev Cell. 2014;31(6):761–73. https://doi.org/10.1016/j.devcel.2014.11.021 PMID: 25535918
19. Arbeitman MN, New FN, Fear JM, Howard TS, Dalton JE, Graze RM. Sex differences in *Drosophila* somatic gene expression: variation and regulation by doublesex. G3 (Bethesda). 2016;6(7):1799–808. https://doi.org/10.1534/g3.116.027961 PMID: 27172187
20. Williams TM, Selegue JE, Werner T, Gompel N, Kopp A, Carroll SB. The regulation and evolution of a genetic switch controlling sexually dimorphic traits in *Drosophila*. Cell. 2008;134(4):610–23. https://doi.org/10.1016/j.cell.2008.06.052 PMID: 18724934
21. Kopp A, Duncan I, Godt D, Carroll SB. Genetic control and evolution of sexually dimorphic characters in *Drosophila*. Nature. 2000;408(6812):553–9. https://doi.org/10.1038/35046017 PMID: 11117736
22. Rutowski RL, Macedonia JM, Merry JW, Morehouse NI, Yturralde K, Taylor-Taft L, et al. Iridescent ultraviolet signal in the orange sulphur butterfly (*Colias eurytheme*): spatial, temporal and spectral properties. Biological Journal of the Linnean Society. 2007;90(2):349–64. https://doi.org/10.1111/j.1095-8312.2007.00749.x
23. Ficarrotta V, Martin A, Counterman BA, Pyron RA. Early origin and diverse phenotypic implementation of iridescent UV patterns for sexual signaling in pierid butterflies. Evolution. 2023;77(12):2619–30. https://doi.org/10.1093/evolut/qpad174 PMID: 37797261
24. Tunström K, Woronik A, Hanly JJ, Rastas P, Chichvarkhin A, Warren AD, et al. Evidence for a single, ancient origin of a genus-wide alternative life history strategy. Sci Adv. 2023;9(12):eabq3713. https://doi.org/10.1126/sciadv.abq3713 PMID: 36947619
25. Woronik A, Neethiraj R, Lehmann P, Maria de la PCM, Stefanescu C, Hill J, et al. A transposable element insertion is associated with a female-limited, alternative life history strategy. 2017 [cited 28 Apr 2024]. Available from: https://www.diva-portal.org/smash/record.jsf?pid=diva2:1144520
26. Hanly JJ, Francescutti CM, Loh LS, Corning OBWH, Long DJ, Nakatani MA, et al. Genetics of yellow-orange color variation in a pair of sympatric sulphur butterflies. Cell Rep. 2023;42(8):112820. https://doi.org/10.1016/j.celrep.2023.112820 PMID: 37481719
27. Silberglied RE, Taylor OR Jr. Ultraviolet reflection and its behavioral role in the courtship of the sulfur butterflies *Colias eurytheme* and *C. philodice* (Lepidoptera, Pieridae). Behav Ecol Sociobiol. 1978;3(3):203–43. https://doi.org/10.1007/bf00296311
28. Silberglied RE, Taylor OR. Ultraviolet differences between the Sulphur Butterflies, *Colias eurytheme* and *C. philodice*, and a possible isolating mechanism. Nature. 1973;241(5389):406–8. https://doi.org/10.1038/241406a0 PMID: 25522436
29. Ficarrotta V, Hanly JJ, Loh LS, Francescutti CM, Ren A, Tunström K, et al. A genetic switch for male UV iridescence in an incipient species pair of sulphur butterflies. Proc Natl Acad Sci U S A. 2022;119(3):e2109255118. https://doi.org/10.1073/pnas.2109255118 PMID: 35012980
30. Kemp DJ, Rutowski RL. The role of coloration in mate choice and sexual interactions in butterflies. Adv Stud Behav. Elsevier. 2011. p. 55–92. https://doi.org/10.1016/b978-0-12-380896-7.00002-2
31. Vasas V, Lowell MC, Villa J, Jamison QD, Siegle AG, Katta PKR, et al. Recording animal-view videos of the natural world using a novel camera system and software package. PLoS Biol. 2024;22(1):e3002444. https://doi.org/10.1371/journal.pbio.3002444 PMID: 38261631
32. Lai EC, Orgogozo V. A hidden program in *Drosophila* peripheral neurogenesis revealed: fundamental principles underlying sensory organ diversity. Dev Biol. 2004;269(1):1–17. https://doi.org/10.1016/j.ydbio.2004.01.032 PMID: 15081353
33. Bardin AJ, Le Borgne R, Schweisguth F. Asymmetric localization and function of cell-fate determinants: a fly's view. Curr Opin Neurobiol. 2004;14(1):6–14. https://doi.org/10.1016/j.conb.2003.12.002 PMID: 15018932
34. Galant R, Skeath JB, Paddock S, Lewis DL, Carroll SB. Expression pattern of a butterfly achaete-scute homolog reveals the homology of butterfly wing scales and insect sensory bristles. Curr Biol. 1998;8(14):807–13. https://doi.org/10.1016/s0960-9822(98)70322-7 PMID: 9663389
35. Pomerantz AF. Making it clear: evolution, development and genetic basis of wing transparency in Lepidoptera. University of California, Berkeley. 2021. Available from: https://search.proquest.com/openview/4c4808e8bcebc94be4adf65ec7cd5880/1?pq-origsite=gscholar&cbl=18750&diss=y&casa_token=IpnAg1hU1wsAAAAA:bX1-Zf4GvI32JIVJ2omblF0DC2xm_znzl3jsE53OijkMGovOZ9prl9We1t1_rOCoznzEDl3O
36. Prakash A, Dion E, Banerjee TD, Monteiro A. The molecular basis of scale development highlighted by a single-cell atlas of *Bicyclus anynana* butterfly pupal forewings. Cell Rep. 2024;43(5):114147. https://doi.org/10.1016/j.celrep.2024.114147 PMID: 38662541

37. Loh LS, DeMarr KA, Tsimba M, Heryanto C, Berrio A, Patel NH, et al. Lepidopteran scale cells derive from sensory organ precursors through a canonical lineage. Development. 2025;152(5):DEV204501. https://doi.org/10.1242/dev.204501 PMID: 40052482
38. Cho EH, Nijhout HF. Development of polyploidy of scale-building cells in the wings of *Manduca sexta*. Arthropod Struct Dev. 2013;42(1):37–46. https://doi.org/10.1016/j.asd.2012.09.003 PMID: 23017249
39. Dinwiddie A, Null R, Pizzano M, Chuong L, Leigh Krup A, Ee Tan H, et al. Dynamics of F-actin prefigure the structure of butterfly wing scales. Dev Biol. 2014;392(2):404–18. https://doi.org/10.1016/j.ydbio.2014.06.005 PMID: 24930704
40. McDougal AD, Kang S, Yaqoob Z, So PTC, Kolle M. In vivo visualization of butterfly scale cell morphogenesis in *Vanessa cardui*. Proc Natl Acad Sci U S A. 2021;118(49):e2112009118. https://doi.org/10.1073/pnas.2112009118 PMID: 34845021
41. Iwata M, Ohno Y, Otaki JM. Real-time in vivo imaging of butterfly wing development: revealing the cellular dynamics of the pupal wing tissue. PLoS One. 2014;9(2):e89500. https://doi.org/10.1371/journal.pone.0089500 PMID: 24586829
42. Ohno Y, Otaki JM. Live cell imaging of butterfly pupal and larval wings in vivo. PLoS One. 2015;10(6):e0128332. https://doi.org/10.1371/journal.pone.0128332 PMID: 26107809
43. Tsai C-C, Childers RA, Nan Shi N, Ren C, Pelaez JN, Bernard GD, et al. Physical and behavioral adaptations to prevent overheating of the living wings of butterflies. Nat Commun. 2020;11(1):551. https://doi.org/10.1038/s41467-020-14408-8 PMID: 31992708
44. Ghiradella H. Development of ultraviolet-reflecting butterfly scales: How to make an interference filter. J Morphol. 1974;142(4):395–409. https://doi.org/10.1002/jmor.1051420404 PMID: 30314406
45. Ghiradella H. Hairs, bristles, and scales. Microscopic anatomy of invertebrates. Insecta. 1998;11A:257–87.
46. Kolyer JM, Reimschuessel AM. Scanning electron microscopy on wing scales of *Colias erytheme*. J Res Lepidoptera. 1969;8(1):1–15. https://doi.org/10.5962/p.333543
47. Rutowski RL. Male scent-producing structures in *Colias* butterflies. J Chem Ecol. 1980;6(1):13–26. https://doi.org/10.1007/bf00987523
48. Rohner PT, Linz DM, Moczek AP. Doublesex mediates species-, sex-, environment- and trait-specific exaggeration of size and shape. Proc Biol Sci. 2021;288(1953):20210241. https://doi.org/10.1098/rspb.2021.0241 PMID: 34157867
49. Hull JJ, Heu CC, Gross RJ, LeRoy DM, Schutze IX, Langhorst D, et al. Doublesex is essential for masculinization but not feminization in *Lygus hesperus*. Insect Biochem Mol Biol. 2024;166:104085. https://doi.org/10.1016/j.ibmb.2024.104085 PMID: 38307215
50. Wang Y, Sun W, Fleischmann S, Millar JG, Ruther J, Verhulst EC. Silencing Doublesex expression triggers three-level pheromonal feminization in *Nasonia vitripennis* males. Proc Biol Sci. 2022;289(1967):20212002. https://doi.org/10.1098/rspb.2021.2002 PMID: 35078369
51. Hammond A, Galizi R, Kyrou K, Simoni A, Siniscalchi C, Katsanos D, et al. A CRISPR-Cas9 gene drive system targeting female reproduction in the malaria mosquito vector *Anopheles gambiae*. Nat Biotechnol. 2016;34(1):78–83. https://doi.org/10.1038/nbt.3439 PMID: 26641531
52. Takahashi M, Okude G, Futahashi R, Takahashi Y, Kawata M. The effect of the doublesex gene in body colour masculinization of the damselfly *Ischnura senegalensis*. Biol Lett. 2021;17(6):20200761. https://doi.org/10.1098/rsbl.2020.0761 PMID: 34102071
53. Komata S, Lin CP, Fujiwara H. Doublesex controls both hindwing and abdominal mimicry traits in the female-limited batesian mimicry of *Papilio memnon*. Frontiers in Insect Science. 2022;20.
54. Iijima T, Yoda S, Fujiwara H. The mimetic wing pattern of *Papilio polytes* butterflies is regulated by a doublesex-orchestrated gene network. Commun Biol. 2019;2:257. https://doi.org/10.1038/s42003-019-0510-7 PMID: 31312726
55. Martin A, McCulloch KJ, Patel NH, Briscoe AD, Gilbert LE, Reed RD. Multiple recent co-options of Optix associated with novel traits in adaptive butterfly wing radiations. Evodevo. 2014;5(1):7. https://doi.org/10.1186/2041-9139-5-7 PMID: 24499528
56. Kunte K, Zhang W, Tenger-Trolander A, Palmer DH, Martin A, Reed RD, et al. Doublesex is a mimicry supergene. Nature. 2014;507(7491):229–32. https://doi.org/10.1038/nature13112 PMID: 24598547
57. Mellert DJ, Robinett CC, Baker BS. Doublesex functions early and late in gustatory sense organ development. PLoS One. 2012;7(12):e51489. https://doi.org/10.1371/journal.pone.0051489 PMID: 23240029
58. Diaz-de-la-Loza M-D-C, Ray RP, Ganguly PS, Alt S, Davis JR, Hoppe A, et al. Apical and basal matrix remodeling control epithelial morphogenesis. Dev Cell. 2018;46(1):23-39.e5. https://doi.org/10.1016/j.devcel.2018.06.006 PMID: 29974861
59. Ghabrial AS, Levi BP, Krasnow MA. A systematic screen for tube morphogenesis and branching genes in the *Drosophila* tracheal system. PLoS Genet. 2011;7(7):e1002087. https://doi.org/10.1371/journal.pgen.1002087 PMID: 21750678
60. Adler PN. A cytoskeletal activator and inhibitor are downstream targets of the frizzled/starry night planar cell polarity pathway in the *Drosophila* epidermis. Prog Biophys Mol Biol. 2018;137:69–75. https://doi.org/10.1016/j.pbiomolbio.2018.04.001 PMID: 29649492
61. Ramírez-Moreno M, Hunton R, Strutt D, Bulgakova NA. Deciphering the roles of cell shape and Fat and Dachsous planar polarity in arranging the *Drosophila* apical microtubule network through quantitative image analysis. Mol Biol Cell. 2023;34(6):ar55. https://doi.org/10.1091/mbc.E22-09-0442 PMID: 36735484
62. Jacobs J, Atkins M, Davie K, Imrichova H, Romanelli L, Christiaens V, et al. The transcription factor Grainy head primes epithelial enhancers for spatiotemporal activation by displacing nucleosomes. Nat Genet. 2018;50(7):1011–20. https://doi.org/10.1038/s41588-018-0140-x PMID: 29867222

63. Nussbaumer U, Halder G, Groppe J, Affolter M, Montagne J. Expression of the blistered/DSRF gene is controlled by different morphogens during *Drosophila* trachea and wing development. Mech Dev. 2000;96(1):27–36. https://doi.org/10.1016/s0925-4773(00)00373-7 PMID: 10940622

64. Weaver TA, White RA. Headcase, an imaginal specific gene required for adult morphogenesis in *Drosophila melanogaster*. Development. 1995;121(12):4149–60. https://doi.org/10.1242/dev.121.12.4149 PMID: 8575315

65. Wang S, Samakovlis C. Grainy head and its target genes in epithelial morphogenesis and wound healing. Curr Top Dev Biol. 2012;98:35–63. https://doi.org/10.1016/B978-0-12-386499-4.00002-1 PMID: 22305158

66. Li Y, Lu T, Dong P, Chen J, Zhao Q, Wang Y, et al. A single-cell atlas of *Drosophila* trachea reveals glycosylation-mediated Notch signaling in cell fate specification. Nat Commun. 2024;15(1):2019. https://doi.org/10.1038/s41467-024-46455-w PMID: 38448482

67. Peng D, Jackson D, Palicha B, Kernfeld E, Laughner N, Shoemaker A, et al. Organogenetic transcriptomes of the *Drosophila* embryo at single cell resolution. Development. 2024;151(2):dev202097. https://doi.org/10.1242/dev.202097 PMID: 38174902

68. Matsuda R, Hosono C, Samakovlis C, Saigo K. Multipotent versus differentiated cell fate selection in the developing *Drosophila* airways. Elife. 2015;4:e09646.

69. Chen F, Krasnow MA. Progenitor outgrowth from the niche in *Drosophila* trachea is guided by FGF from decaying branches. Science. 2014;343(6167):186–9. https://doi.org/10.1126/science.1241442

70. Hopkins BR, Barmina O, Kopp A. A single-cell atlas of the sexually dimorphic *Drosophila* foreleg and its sensory organs during development. PLoS Biol. 2023;21(6):e3002148. https://doi.org/10.1371/journal.pbio.3002148 PMID: 37379332

71. Miller SW, Avidor-Reiss T, Polyanovsky A, Posakony JW. Complex interplay of three transcription factors in controlling the tormogen differentiation program of *Drosophila* mechanoreceptors. Dev Biol. 2009;329(2):386–99. https://doi.org/10.1016/j.ydbio.2009.02.009 PMID: 19232522

72. Kavaler J, Fu W, Duan H, Noll M, Posakony JW. An essential role for the *Drosophila* Pax2 homolog in the differentiation of adult sensory organs. Development. 1999;126(10):2261–72. https://doi.org/10.1242/dev.126.10.2261 PMID: 10207150

73. Johnson SA, Harmon KJ, Smiley SG, Still FM, Kavaler J. Discrete regulatory regions control early and late expression of D-Pax2 during external sensory organ development. Dev Dyn. 2011;240(7):1769–78. https://doi.org/10.1002/dvdy.22672 PMID: 21644243

74. Abdelilah-Seyfried S, Chan YM, Zeng C, Justice NJ, Younger-Shepherd S, Sharp LE, et al. A gain-of-function screen for genes that affect the development of the *Drosophila* adult external sensory organ. Genetics. 2000;155(2):733–52. https://doi.org/10.1093/genetics/155.2.733 PMID: 10835395

75. Sun Z, Inagaki S, Miyoshi K, Saito K, Hayashi S. Osiris gene family defines the cuticle nanopatterns of *Drosophila*. Genetics. 2024;227(2):iyae065. https://doi.org/10.1093/genetics/iyae065 PMID: 38652268

76. Derivery E, Seum C, Daeden A, Loubéry S, Holtzer L, Jülicher F, et al. Polarized endosome dynamics by spindle asymmetry during asymmetric cell division. Nature. 2015;528: 280–85. Available from: https://idp.nature.com/authorize/casa?redirect_uri= https://www.nature.com/articles/nature16443&casa_token=7nsLy6Re6AkAAAAA:cCiwAJ5nWZefFHhjWxFGjYduaYwCMobe6_optOVwKCxS4aofkoFChnJJYEQoAtKc3KG8XA3Z-Djorfg

77. Shalaby NA, Parks AL, Morreale EJ, Osswalt MC, Pfau KM, Pierce EL, et al. A screen for modifiers of notch signaling uncovers Amun, a protein with a critical role in sensory organ development. Genetics. 2009;182(4):1061–76. https://doi.org/10.1534/genetics.108.099986 PMID: 19448274

78. Loh LS, Martin A. Data for: single-nucleus transcriptomic signatures of wing sexual dimorphism and scale cell specialization in sulphur butterflies. OSF. 2024. https://doi.org/10.17605/OSF.IO/YJVKC

79. Prakash A, Monteiro A. apterous A specifies dorsal wing patterns and sexual traits in butterflies. Proc Biol Sci. 2018;285(1873):20172685. https://doi.org/10.1098/rspb.2017.2685 PMID: 29467265

80. Hanly JJ, Wallbank RWR, McMillan WO, Jiggins CD. Conservation and flexibility in the gene regulatory landscape of heliconiine butterfly wings. Evodevo. 2019;10:15. https://doi.org/10.1186/s13227-019-0127-4 PMID: 31341608

81. Prakash A, Finet C, Banerjee TD, Saranathan V, Monteiro A. Antennapedia and optix regulate metallic silver wing scale development and cell shape in *Bicyclus anynana* butterflies. Cell Rep. 2022;40(1):111052. https://doi.org/10.1016/j.celrep.2022.111052 PMID: 35793633

82. Chatterjee M, Yu XY, Brady NK, Hatto GC, Reed RD. Mirror determines the far posterior domain in butterfly wings. eLife Sciences Publications, Ltd. 2024. https://doi.org/10.7554/elife.96904.1

83. Macdonald WP, Martin A, Reed RD. Butterfly wings shaped by a molecular cookie cutter: evolutionary radiation of lepidopteran wing shapes associated with a derived Cut/wingless wing margin boundary system. Evol Dev. 2010;12(3):296–304. https://doi.org/10.1111/j.1525-142X.2010.00415.x PMID: 20565540

84. Livraghi L, Hanly JJ, Evans E, Wright CJ, Loh LS, Mazo-Vargas A, et al. A long noncoding RNA at the cortex locus controls adaptive coloration in butterflies. Proc Natl Acad Sci U S A. 2024;121(36):e2403326121. https://doi.org/10.1073/pnas.2403326121 PMID: 39213180

85. Zhang L, Martin A, Perry MW, van der Burg KRL, Matsuoka Y, Monteiro A, et al. Genetic basis of melanin pigmentation in butterfly wings. Genetics. 2017;205(4):1537–50. https://doi.org/10.1534/genetics.116.196451 PMID: 28193726

86. Fandino RA, Brady NK, Chatterjee M, McDonald JMC, Livraghi L, van der Burg KRL, et al. The ivory lncRNA regulates seasonal color patterns in buckeye butterflies. Proc Natl Acad Sci U S A. 2024;121(41):e2403426121. https://doi.org/10.1073/pnas.2403426121 PMID: 39352931

87. Tian S, Asano Y, Das Banerjee T, Komata S, Wee JLQ, Lamb A, et al. A microRNA is the effector gene of a classic evolutionary hotspot locus. Science. 2024;386(6726):1135–41. https://doi.org/10.1126/science.adp7899 PMID: 39636974

88. Banerjee TD, Murugesan SN, Connahs H, Monteiro A. Spatial and temporal regulation of Wnt signaling pathway members in the development of butterfly wing patterns. Sci Adv. 2023;9(30):eadg3877. https://doi.org/10.1126/sciadv.adg3877 PMID: 37494447

89. Hanly JJ, Loh LS, Mazo-Vargas A, Rivera-Miranda TS, Livraghi L, Tendolkar A, et al. Frizzled2 receives WntA signaling during butterfly wing pattern formation. Development. 2023;150(18):dev201868. https://doi.org/10.1242/dev.201868 PMID: 37602496

90. Suzuki MG, Imanishi S, Dohmae N, Asanuma M, Matsumoto S. Identification of a male-specific RNA binding protein that regulates sex-specific splicing of Bmdsx by increasing RNA binding activity of BmPSI. Mol Cell Biol. 2010;30(24):5776–86. https://doi.org/10.1128/MCB.00444-10 PMID: 20956562

91. Lours C, Bardot O, Godt D, Laski FA, Couderc J-L. The Drosophila melanogaster BTB proteins bric à brac bind DNA through a composite DNA binding domain containing a pipsqueak and an AT-Hook motif. Nucleic Acids Res. 2003;31(18):5389–98. https://doi.org/10.1093/nar/gkg724 PMID: 12954775

92. Pointud JC, Larsson J, Dastugue B, Couderc JL. The BTB/POZ domain of the regulatory proteins Bric à brac 1 (BAB1) and Bric à brac 2 (BAB2) interacts with the novel *Drosophila* TAF(II) factor BIP2/dTAF(II)155. Dev Biol. 2001;237(2):368–80. https://doi.org/10.1006/dbio.2001.0358 PMID: 11543621

93. Chaharbakhshi E, Jemc JC. Broad-complex, tramtrack, and bric-à-brac (BTB) proteins: critical regulators of development. Genesis. 2016;54(10):505–18. https://doi.org/10.1002/dvg.22964 PMID: 27521773

94. VanKuren NW, Sheikh SI, Massardo D, Lu W, Kronforst MR. Supergene evolution via gain of auto-regulation. bioRxiv. 2024.

95. Aase-Remedios ME, Janssen R, Leite DJ, Sumner-Rooney L, McGregor AP. Evolution of the spider homeobox gene repertoire by tandem and whole genome duplication. Mol Biol Evol. 2023;40(12):msad239. https://doi.org/10.1093/molbev/msad239 PMID: 37935059

96. Behr M, Hoch M. Identification of the novel evolutionary conserved obstructor multigene family in invertebrates. FEBS Lett. 2005;579(30):6827–33. https://doi.org/10.1016/j.febslet.2005.11.021 PMID: 16325182

97. Petkau G, Wingen C, Jussen LCA, Radtke T, Behr M. Obstructor-A is required for epithelial extracellular matrix dynamics, exoskeleton function, and tubulogenesis. J Biol Chem. 2012;287(25):21396–405. https://doi.org/10.1074/jbc.M112.359984 PMID: 22544743

98. Tajiri R, Ogawa N, Fujiwara H, Kojima T. Mechanical control of whole body shape by a single cuticular protein obstructor-E in *Drosophila melanogaster*. PLOS Genetics. 2017;13: e1006548. https://doi.org/10.1371/journal.pgen.1006548

99. Alachiotis N, Pavlidis P. RAiSD detects positive selection based on multiple signatures of a selective sweep and SNP vectors. Commun Biol. 2018;1:79. https://doi.org/10.1038/s42003-018-0085-8 PMID: 30271960

100. Tilney LG, Connelly PS, Ruggiero L, Vranich KA, Guild GM, Derosier D. The role actin filaments play in providing the characteristic curved form of *Drosophila* bristles. Mol Biol Cell. 2004;15(12):5481–91. https://doi.org/10.1091/mbc.e04-06-0472 PMID: 15371540

101. Hammonds AS, Fristrom JW. Mutational analysis of Stubble-stubbloid gene structure and function in *Drosophila* leg and bristle morphogenesis. Genetics. 2006;172(3):1577–93. https://doi.org/10.1534/genetics.105.047100 PMID: 16322506

102. Koch N, Dharmalingam E, Westermann M, Qualmann B, Thomas U, Kessels MM. Abp1 utilizes the Arp2/3 complex activator Scar/WAVE in bristle development. J Cell Sci. 2012;125(Pt 15):3578–89. https://doi.org/10.1242/jcs.101451 PMID: 22467854

103. Monteiro A, Glaser G, Stockslager S, Glansdorp N, Ramos D. Comparative insights into questions of lepidopteran wing pattern homology. BMC Dev Biol. 2006;6:52. https://doi.org/10.1186/1471-213X-6-52 PMID: 17090321

104. Wee JLQ, Das Banerjee T, Prakash A, Seah KS, Monteiro A. Distal-less and spalt are distal organisers of pierid wing patterns. Evodevo. 2022;13(1):12. https://doi.org/10.1186/s13227-022-00197-2 PMID: 35659745

105. Wee JLQ, Murugesan SN, Wheat CW, Monteiro A. The genetic basis of wing spots in *Pieris canidia* butterflies. BMC Genomics. 2023;24(1):169. https://doi.org/10.1186/s12864-023-09261-0 PMID: 37016295

106. Stoehr AM, Walker JF, Monteiro A. Spalt expression and the development of melanic color patterns in pierid butterflies. Evodevo. 2013;4(1):6. https://doi.org/10.1186/2041-9139-4-6 PMID: 23419038

107. Fenner J, Benson C, Rodriguez-Caro L, Ren A, Papa R, Martin A. Wnt genes in wing pattern development of Coliadinae butterflies. Front Ecol Evol. 2020;8:00197.

108. Rougeot J, Guerra F, Verhulst EC. A transcriptional control model for doublesex-dependent sex differentiation in Nasonia wasps. bioRxiv. 2025; 2025–02. Available from: https://www.biorxiv.org/content/10.1101/2025.02.03.636189.abstract

109. Ledón-Rettig CC, Zattara EE, Moczek AP. Asymmetric interactions between doublesex and tissue- and sex-specific target genes mediate sexual dimorphism in beetles. Nat Commun. 2017;8:14593. https://doi.org/10.1038/ncomms14593 PMID: 28239147

110. Roeske MJ, Camino EM, Grover S, Rebeiz M, Williams TM. Cis-regulatory evolution integrated the Bric-à-brac transcription factors into a novel fruit fly gene regulatory network. Elife. 2018;7:e32273. https://doi.org/10.7554/eLife.32273 PMID: 29297463

111. Rogers WA, Salomone JR, Tacy DJ, Camino EM, Davis KA, Rebeiz M, et al. Recurrent modification of a conserved cis-regulatory element underlies fruit fly pigmentation diversity. PLoS Genet. 2013;9(8):e1003740. https://doi.org/10.1371/journal.pgen.1003740 PMID: 24009528

112. van der Bijl W, Zeuss D, Chazot N, Tunström K, Wahlberg N, Wiklund C, et al. Butterfly dichromatism primarily evolved via Darwin's, not Wallace's, model. Evolution letters. 2020;4: 545–555. Available: https://academic.oup.com/evlett/article-abstract/4/6/545/6697558

113. Stella D, Faltýnek Fric Z, Rindoš M, Kleisner K, Pechácek P. Distribution of ultraviolet ornaments in *Colias* butterflies (Lepidoptera: Pieridae). Environ Entomol. 2018;47(5):1344–54. https://doi.org/10.1093/ee/nvy111 PMID: 30085041

114. Rodriguez-Caro F, Fenner J, Bhardwaj S, Cole J, Benson C, Colombara AM, et al. Novel doublesex duplication associated with sexually dimorphic development of dogface butterfly wings. Mol Biol Evol. 2021;38(11):5021–33. https://doi.org/10.1093/molbev/msab228 PMID: 34323995

115. 2Kottler MJ. Darwin, Wallace, and the origin of sexual dimorphism. Proc Am Philos Soc. 1980;124(3):203–26. PMID: 11615818

116. Allen CE, Zwaan BJ, Brakefield PM. Evolution of sexual dimorphism in the Lepidoptera. Annu Rev Entomol. 2011;56:445–64. https://doi.org/10.1146/annurev-ento-120709-144828 PMID: 20822452

117. Lande R. Sexual dimorphism, sexual selection, and adaptation in polygenic characters. Evolution. 1980;34(2):292. https://doi.org/10.2307/2407393

118. Wedell N, Kemp DJ. Ultraviolet signaling in a butterfly is preferred by females and conveys male genetic quality. Evolution. 2024;78(8):1372–81. https://doi.org/10.1093/evolut/qpae080 PMID: 38776186

119. Ödeen A, Håstad O. The phylogenetic distribution of ultraviolet sensitivity in birds. BMC Evol Biol. 2013;13:36. https://doi.org/10.1186/1471-2148-13-36 PMID: 23394614

120. Ghiradella H, Aneshansley D, Eisner T, Silberglied RE, Hinton HE. Ultraviolet reflection of a male butterfly: interference color caused by thin-layer elaboration of wing scales. Science. 1972;178(4066):1214–7. https://doi.org/10.1126/science.178.4066.1214 PMID: 17748984

121. Day CR, Hanly JJ, Ren A, Martin A. Sub-micrometer insights into the cytoskeletal dynamics and ultrastructural diversity of butterfly wing scales. Dev Dyn. 2019.

122. Seah KS, Saranathan V. Hierarchical morphogenesis of swallowtail butterfly wing scale nanostructures. Elife. 2023;12:RP89082. https://doi.org/10.7554/eLife.89082 PMID: 37768710

123. Lloyd VJ, Burg SL, Harizanova J, Garcia E, Hill O, Enciso-Romero J, et al. The actin cytoskeleton plays multiple roles in structural colour formation in butterfly wing scales. Nat Commun. 2024;15(1):4073. https://doi.org/10.1038/s41467-024-48060-3 PMID: 38769302

124. Ren N, He B, Stone D, Kirakodu S, Adler PN. The shavenoid gene of *Drosophila* encodes a novel actin cytoskeleton interacting protein that promotes wing hair morphogenesis. Genetics. 2006;172(3):1643–53. https://doi.org/10.1534/genetics.105.051433 PMID: 16322503

125. Guild GM, Connelly PS, Ruggiero L, Vranich KA, Tilney LG. Actin filament bundles in *Drosophila* wing hairs: hairs and bristles use different strategies for assembly. Mol Biol Cell. 2005;16(8):3620–31. https://doi.org/10.1091/mbc.e05-03-0185 PMID: 15917291

126. Wang S, Jayaram SA, Hemphälä J, Senti K-A, Tsarouhas V, Jin H, et al. Septate-junction-dependent luminal deposition of chitin deacetylases restricts tube elongation in the *Drosophila* trachea. Curr Biol. 2006;16(2):180–5. https://doi.org/10.1016/j.cub.2005.11.074 PMID: 16431370

127. Karouzou MV, Spyropoulos Y, Iconomidou VA, Cornman RS, Hamodrakas SJ, Willis JH. *Drosophila* cuticular proteins with the R&R Consensus: annotation and classification with a new tool for discriminating RR-1 and RR-2 sequences. Insect Biochem Mol Biol. 2007;37:754–60. Available from: https://www.sciencedirect.com/science/article/pii/S0965174807000653?casa_token=UqzF5pXT6vQAAAAA:aQnrLT9tEG88mpHZFbHN-vHXQqQT7jA9bbtqogX116cwwfmMaLRJxW02gahT3fBn3p1Iq8y8

128. Fujiwara H, Nishikawa H. Functional analysis of genes involved in color pattern formation in Lepidoptera. Curr Opin Insect Sci. 2016;17:16–23. https://doi.org/10.1016/j.cois.2016.05.015 PMID: 27720069

129. Ebdon S, Mackintosh A, Hayward A, Wotton K, et al.; Darwin Tree of Life Barcoding collective, Wellcome Sanger Institute Tree of Life programme. The genome sequence of the clouded yellow, *Colias crocea* (Geoffroy, 1785). Wellcome Open Res. 2021;6:284. https://doi.org/10.12688/wellcomeopenres.17292.1 PMID: 36157970

130. Shumate A, Salzberg SL. Liftoff: accurate mapping of gene annotations. Bioinformatics. 2021;37(12):1639–43. https://doi.org/10.1093/bioinformatics/btaa1016 PMID: 33320174

131. McLaughlin CN, Qi Y, Quake SR, Luo L, Li H. Isolation and RNA sequencing of single nuclei from *Drosophila* tissues. STAR Protoc. 2022;3:101417. https://doi.org/10.1016/j.xpro.2022.101417

132. Gu Z. Complex heatmap visualization. Imeta. 2022;1(3):e43. https://doi.org/10.1002/imt2.43 PMID: 38868715

133. Gu Z, Eils R, Schlesner M. Complex heatmaps reveal patterns and correlations in multidimensional genomic data. Bioinformatics. 2016;32(18):2847–9. https://doi.org/10.1093/bioinformatics/btw313 PMID: 27207943

134. Landt SG, Marinov GK, Kundaje A, Kheradpour P, Pauli F, Batzoglou S, et al. ChIP-seq guidelines and practices of the ENCODE and modENCODE consortia. Genome Res. 2012;22(9):1813–31. https://doi.org/10.1101/gr.136184.111 PMID: 22955991

135. Li Q, Brown JB, Huang H, Bickel PJ. Measuring reproducibility of high-throughput experiments. 2011 [cited 5 Aug 2024]. Available from: https://projecteuclid.org/journals/annals-of-applied-statistics/volume-5/issue-3/Measuring-reproducibility-of-high-throughput/10.1214/11-AOAS466.short

136. Heinz S, Benner C, Spann N, Bertolino E, Lin YC, Laslo P, et al. Simple combinations of lineage-determining transcription factors prime *cis*-regulatory elements required for macrophage and B cell identities. Mol cell. 2010;38: 576–89. Available from: https://www.cell.com/molecular-cell/pdf/S1097-2765(10)00366-7.pdf

137. Ramírez F, Ryan DP, Grüning B, Bhardwaj V, Kilpert F, Richter AS, et al. deepTools2: a next generation web server for deep-sequencing data analysis. Nucleic Acids Res. 2016;44(W1):W160-5. https://doi.org/10.1093/nar/gkw257 PMID: 27079975

138. Machanick P, Bailey TL. MEME-ChIP: motif analysis of large DNA datasets. Bioinformatics. 2011;27(12):1696–7. https://doi.org/10.1093/bioinformatics/btr189 PMID: 21486936

**139.** Averof M, Cohen SM. Evolutionary origin of insect wings from ancestral gills. Nature. 1997;385:627–30. Available from: https://idp.nature.com/authorize/casa?redirect_uri= https://www.nature.com/articles/385627a0&casa_token=aAgtlBsuPV8AAAAA:KlegGQqH_N17lt7C9hBWDqmGe18_BkV405gzwSEPqy77QnNdXdJeOykQELowa7uwOm30ziQSk3Pixg

**140.** Blochlinger K, Bodmer R, Jan LY, Jan YN. Patterns of expression of cut, a protein required for external sensory organ development in wild-type and cut mutant *Drosophila* embryos. Genes Dev. 1990;4(8):1322–31. https://doi.org/10.1101/gad.4.8.1322 PMID: 1977661

**141.** Glicksman MA, Brower DL. Misregulation of homeotic gene expression in *Drosophila* larvae resulting from mutations at the extra sex combs locus. Dev Biol. 1988;126(2):219–27. https://doi.org/10.1016/0012-1606(88)90132-7 PMID: 2895027

**142.** Perry M, Kinoshita M, Saldi G, Huo L, Arikawa K, Desplan C. Molecular logic behind the three-way stochastic choices that expand butterfly colour vision. Nature. 2016;535(7611):280–4. https://doi.org/10.1038/nature18616 PMID: 27383790